ADVANCED ENGINEERING MATERIALS

REVIEW

DOI: 10.1002/adem.201300409

Field-Assisted Sintering Technology/ Spark Plasma Sintering: Mechanisms, Materials, and Technology Developments**

By *Olivier Guillon,* Jesus Gonzalez-Julian, Benjamin Dargatz, Tobias Kessel, Gabi Schierning, Jan Räthel* and *Mathias Herrmann*

Field-assisted sintering technology/Spark plasma sintering is a low voltage, direct current (DC) pulsed current activated, pressure-assisted sintering, and synthesis technique, which has been widely applied for materials processing in the recent years. After a description of its working principles and historical background, mechanical, thermal, electrical effects in FAST/SPS are presented along with the role of atmosphere. A selection of successful materials development including refractory materials, nanocrystalline functional ceramics, graded, and non-equilibrium materials is then discussed. Finally, technological aspects (advanced tool concepts, temperature measurement, finite element simulations) are covered.

1. Introduction

1.1. Definition

The field-assisted sintering technique/Spark plasma sintering (FAST/SPS) is a low voltage, direct current (DC) pulsed current activated, pressure-assisted sintering, and synthesis technique.[1–4] This method can indeed be used to synthesize new compounds[5,6] and/or to densify materials in one step. FAST/SPS is similar to hot pressing (HP), but the way the heat is produced and transmitted to the sintering material is different. If the green body is electrically conductive, energy is dissipated directly within the sample and the electrically

[*] *Prof. O. Guillon[+], Dr. J. Gonzalez-Julian, B. Dargatz*
Otto Schott Institute of Materials Research, Friedrich Schiller University of Jena, Löbdergraben 32, D-07743 Jena, Germany
E-mail: o.guillon@fz-juelich.de
T. Kessel
FCT Systeme GmbH, Rauenstein, Gewerbepark 16, D-96528 Frankenblick, Germany
Dr. G. Schierning
Faculty of Engineering, Center for NanoIntegration Duisburg-Essen (CENIDE), University of Duisburg-Essen, Bismarckstr. 81, D-47057 Duisburg, Germany
J. Räthel, Dr. M. Herrmann
Fraunhofer Institut für keramische Technologien und Systeme (IKTS), Winterbergstr. 28, D-01277 Dresden, Germany
[+] *Present address: Institute of Energy and Climate Research IEK-1: Materials, Synthesis and Processing, Forschungszentrum Jülich and Faculty of Georesources and Materials Engineering, RWTH University, Aachen, Germany*

[**] *This paper was written by members of the new expert committee on FAST/SPS, which is endorsed by the Powder Metallurgy professional organization (FPM), Steel Institute (VDEh), German Engineer Association (VDI-GME), German Ceramic Society (DKG), and German Materials Society (DGM). O. G. acknowledges the financial support of the Materials and Structures Laboratory, Tokyo Institute of Technology, Japan, which hosted him during the preparation of this manuscript. Information provided by J. Huber (Dr Fritsch GmbH) is acknowledged.*

ADVANCED ENGINEERING MATERIALS

conductive parts of the pressing tool. Otherwise, an electrically conductive tool must be used and the heat produced by Joule heating is transmitted by conduction to the powder. The name "Spark plasma sintering" is the most used denomination among a total of 60 found in the literature.[4] However, as no spark or plasma could be detected so far (which is a very difficult task anyway), [7,8] we prefer to add the more general name "field-assisted sintering technique," which also provides a convenient acronym. The common denomination "pulsed electric current sintering" insists upon the non-continuous nature of the electric supply. The adopted appellations do not explicitly mention the role of mechanical pressure, which nevertheless plays a major role in the process, as detailed in Section 2.

Olivier Guillon *After his engineering degree and PhD in France and a research stay at the University of Washington (USA), Olivier Guillon established an Emmy Noether Group funded by the German Research Foundation at the Technische Universität Darmstadt. After 2 years spent at the Friedrich Schiller University of Jena, he is now director at the Institute of Energy and Climate Research – Materials Synthesis and Processing (Forschungszentrum Jülich) as well as professor at the RWTH University Aachen. His interests encompass constrained sintering, field-assisted sintering technology, phase transformation of nanoparticles, solid oxide fuel/electrolytic cells, thermal barrier coatings, gas separation membranes and batteries. His achievements have been recognized at an international level (DGM-Masing Prize, FEMS Materials Science and Technology Prize, R.L. Coble Award of the American Ceramic Society).*

Tobias Kessel *has studied Material Science at the University of Bayreuth, focusing in the field of technical ceramics and fiber-reinforced materials, obtaining his diploma as a graduate engineer in 2006. Being member of the R&D-team at FCT Systeme GmbH in Frankenblick for more than 7 years, he is now working as the product manager of the SPS/FAST-furnaces, responsible for furnace-, process-, and special tool development as well as international furnace start-up and support.*

Jan Räthel *has studied Materials Science focusing on glass and ceramic technology at Technical University of Ilmenau, Germany. He has been working since 2006 on Field Assisted Sintering Technology or Spark Plasma Sintering in the Heat Treatment group at Fraunhofer Institute for Ceramic Technologies and Systems (IKTS). Besides technological aspects of FAST/SPS, scalability, tool design, process optimization (FEM, temperature measurement), and validation are his main fields of interest.*

1.2. Working Principle

FAST/SPS consists of a mechanical loading system, which acts at the same time as high-power electrical circuit, placed in a controlled atmosphere (Figure 1).[9] Thanks to the good electrical conductivity of the materials used for tooling, low voltages (typically below 10 V applied to the whole set-up) produce high currents (typically from 1 to 10 kA) leading to efficient Joule heating (Figure 1). Even in the case of electrically non-conductive sintering powder, heat is quickly and efficiently transferred to the sample. Depending on the used hardware it is possible to define pulse and pause durations or more specialized pulse patterns.[2,10] Typical pulse duration is in the order of a few milliseconds. Owing to the compact geometry of the die and punches, sintering cycles with heating rates as high as 1000 °C min^{-1} are thus possible and enable to significantly reduce the total duration of the process and energy costs.[10] Standard cooling rates up to 150 °C min^{-1} are possible; additional active cooling under gas flow enable to reach quenching rates of 400 °C min^{-1}. At the same time, the simultaneous application of a uniaxial mechanical pressure enhances densification (maximal loads typically between 50 and 250 kN). The process can take place under vacuum or protective gas at atmospheric pressure: all heated parts are kept in a water-cooled chamber. Control of the processing cycle is usually done by temperature measurement (using either thermocouples or axial/radial pyrometers, as detailed in Section 4.3) but can also be achieved by other methods like power-, current-, or simply by displacement control.[9,11] Maximal temperature achieved by using standard graphite tools lies up to 2400 °C.

Whether the sample or the die is heated depends on the electrical resistance of the tool components and the sample material itself (Figure 2). With a conductive sample material,

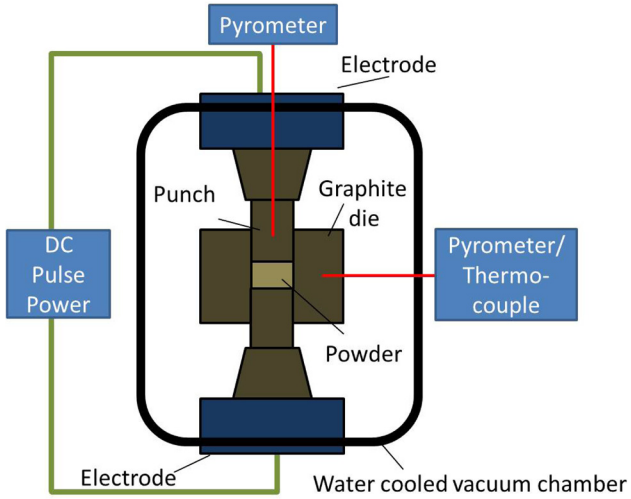

Fig. 1. Working schematic of a FAST apparatus.

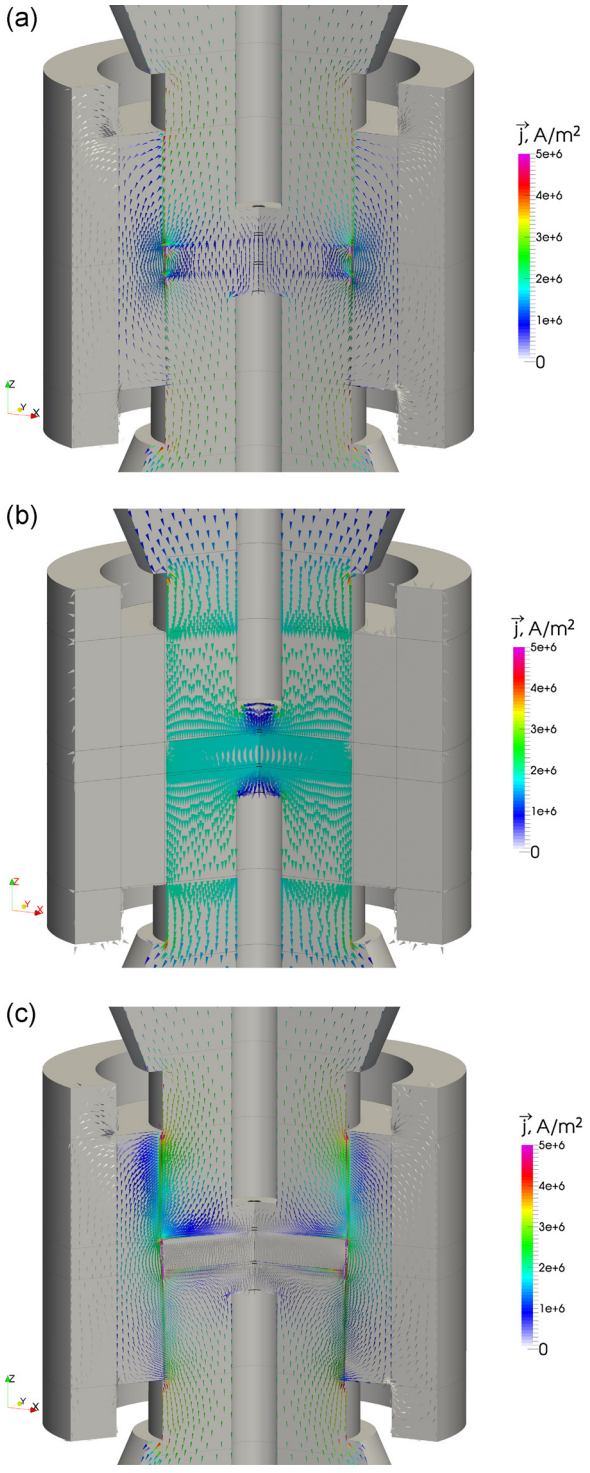

Fig. 2. Schematic current flow in the case of: (a) conductive powder and die, (b) conductive powder, insulating die, (c) non-conductive powder, conductive die (note the vertical hole in the punch to enable temperature measurement by an axial pyrometer).

best results can be achieved when using an electrically insulating die, because the current is forced to go through the material, generating the highest possible current density (Figure 2b). It is possible to sinter non-conductive material (without possible current-assisted sintering mechanisms) creating a heating pattern similar to a rapid HP cycle (Figure 2c). When using a graphite die the current can be forced to go through the sample material by applying electrically insulating coatings as separation layers on the inner surface of the die. Results are then comparable to the setup shown in Figure 2b).

Figure 2 also describes the possible behavior of a composite material consisting of two phases, one being electrically insulating and the other electrically conductive (the amount of the conducting phase below the percolation threshold). The changes in sample's resistivity have dramatic consequences on the current and temperature evolution. As the composite powder starts to sinter, current flows through the die (Figure 2c). As soon as first electrical paths are established, current starts to flow within the sample (Figure 2a). Shortly before reaching full density, the resistivity might drop to very low values so that the sample acts as current sink (Figure 2b).[12]

The resistance of the tool assembly (which can be modified by changing tool dimensions and/or tool material) will have a significant effect on the temperature distribution within the sample and tool too.[13,14] A successful up-scaling to larger sample dimensions or more complex shapes than the typical disc geometry require the use of reliable predictive tools such as finite element modeling as described in Section 4.4.

1.3. Historical Background

If the first mention of sintering under electric current dates back to 1906[15] a US patent deposited in 1913 aimed to protect a pressure- and current-assisted sintering system working in vacuum.[16] More than 50 years later (and about 20 additional patents) Inoue invented the "spark sintering" based on pulsed current, but commercialization did not come to a large success.[17] After Lockheed Missile and Space Co. bought parts of Inoue's work, near-net-shape products, very large components, functionally graded materials (FGMs) and non-equilibrium composites were already produced with this technique in the late 1970s,[18–23] but successful implementation in industry has hardly been documented. After Inoue's patents expired in the early 1990s, Japanese companies (and in particular Sumitomo Coal Mining Co. Ltd) started the industrial production of "Spark Plasma Sintering machines. This explains the predominance of far eastern countries in terms of patents and scientific papers in this engineering field.[24] Later on, FCT Systeme GmbH in Germany and Thermal Technology LLC, Inc. in the USA started producing similar equipment based on pulsed DC current. Nowadays, several companies from China, Korea and Japan offer FAST/SPS set-ups. It is noteworthy to mention that a related technology, using AC current, has been produced since 1953 by a German company (Dr Fritsch GmbH) and is widely used in the diamond composite and hard metal industry. The detailed history of the technical development of electric current activated/assisted sintering can be found in an interesting review.[24] Today, the total number of FAST/SPS devices or equivalent (among them Dr Fritsch GmbH) installed in the world is estimated to 1750 (with 2/3 in the industry). According to the ISI Web of Science, more than 3000

ADVANCED ENGINEERING MATERIALS

papers have been published so far on this technique and its applications, with an exponential growth starting from the 1990s corresponding to the availability of commercial equipment.

2. Mechanisms Involved in FAST/SPS

2.1. Mechanical Effects

The quasi-static compressive stress applied in FAST/SPS leads to a better contact between particles, changes the amount and morphology of those contacts, enhances the existing densification mechanisms already present in free sintering (grain boundary diffusion, lattice diffusion, and viscous flow) or activate new mechanisms, such as plastic deformation or grain boundary sliding.[25] It is not expected to affect the non-densifying mechanisms such as surface diffusion or evaporation/condensation.

Creep equations describing the deformation of dense materials at high temperature were adapted by Coble by taking into account the porous nature of the sintering body. Although simplistic, this continuum mechanical description is useful to identify the main mechanisms during FAST/SPS.[26] The axial shrinkage of the sample is not directly accessible: the total displacement of the machine including elastic and thermal deformations must be calibrated with a dense dummy sample following the same schedule. The normalized densification rate – equal to the opposite of the strain rate – is proportional to the effective stress at the power of stress exponent n. The effective stress is equal to the uniaxial applied stress multiplied by the stress intensification factor. The stress intensification factor describes how the macroscopic applied stress is magnified in a porous body (for a dense material, it is equal to 1). The normalized densification rate is also inversely proportional to the grain size at the power of m (grain size exponent). The values of n and m depend on the sintering mechanism. For diffusion-controlled densification, the strain rate is proportional to the effective stress ($n = 1$). Being a thermally activated process, densification is characterized by the activation energy of the mechanism of matter transport involved. Useful "deformation mechanism maps" have been established showing the controlling densification mechanism based on the temperature, pressure conditions, and grain size.[27,28]

The amplitude of the applied stress is limited by the high-temperature fracture strength of the pressing tool (for graphite, 100–150 MPa) and the loading system. In addition, Salamon *et al.*[29] recorded punch vibrations correlating with pulsed current characteristics. An oscillating stress component may therefore be superimposed to the static component generated by the hydraulic system, possibly enhancing packing at the beginning of sintering in some cases.

Even if grain growth is delayed and reduced under mechanical pressure, it is not totally suppressed. The final grain size can be several times larger than the initial particle size and comparable sintering trajectories have been measured for several oxides densified by FAST/SPS and HP.[30–32] This effect should be particularly marked for agglomerated nanopowders. A finer starting particle size may even lead to a larger grain size than a coarser one at full density.[33] Therefore, a homogeneous green body remains of paramount importance for FAST/SPS when moderate pressures are used. Grain growth stagnation in yttria was attributed to the presence of nanopores at grain junctions.[34] As soon as these pinning points disappear, rapid coarsening take place. On the other hand, as observed for nanocrystalline YAG[35] or $SrTiO_3$,[36] grain coalescence may take place by rotation and sliding of grains, effects which are assisted by the applied pressure. Crystallites seem to align to form lower-angle grain boundaries, which triggers grain boundary migration and end up into larger clusters and massive grain growth. The situation is slightly different for materials, which densify by liquid phase sintering mechanism. As was shown for Si_3N_4-materials nearly complete densification can be achieved by rearrangement accelerated by viscous flow of the liquid with less than 10 vol% of the grains originating from solution-precipitation.[37,38] A similar behavior was found for liquid phase sintered SiC. In liquid-phase-assisted FAST/SPS grain growth can be minimized due to the applied pressure and fast heating, but the liquid phase can be partially squeezed out if its amount is too high or the pressure–time cycles are not selected carefully. The application of the load can also result in texturing if elongated grains are used or form during densification.[39,40] This process is similar to the observed texturing during HP.

By increasing the pressure in FAST/SPS up to several hundreds of MPa, powder agglomerates may break. This particle rearrangement at low temperature increases packing and reduces pore size, allowing homogeneous subsequent densification and limited grain growth. Second, at higher temperature, additional densification mechanisms may be active, including plastic deformation – as the yield stress decreases with temperature – or power-law creep. Consequently, lower temperatures are required for full densification and grain growth is significantly limited. Successful examples of high-pressure FAST/SPS up to 1 GPa will be detailed in Section 3. However, such high-pressure conditions require creep-resistant, tough, and expensive materials such as silicon nitride or tungsten carbide for tooling as well as the reduction of sample cross-section.[41,42] Carbon fiber-reinforced graphite might be a cheaper, easy-to-machine option.[43]

2.2. Thermal Effects

Besides pressure, one definite advantage of FAST/SPS is the availability of high-heating rates. When the dominant densification mechanism (such as grain boundary diffusion) has higher activation energy than the coarsening mechanism (like surface diffusion), reaching rapidly high-sintering temperature can be beneficial to enhance densification rate while retarding microstructure coarsening. In addition, power-law creep in metals can be accelerated for rapid increases of temperature, as shown on aluminum powder.[44]

Independent of the sintering method, for all heating rates considered ranging from a fraction of degree up to several hundreds of degree celsius·per minute, almost fully dense samples which were quickly heated possess a reduced final grain size compared to their slow-heated counterparts[45,46] although some exceptions are possible. For instance drastic grain size reduction was observed on alumina when heating from 50 to 700 °C min^{-1}.[47] As grain growth requires time at high temperature for which grain boundary mobility is enhanced, the shorter the time the sintering body has to be held at maximum temperature, the more coarsening should be suppressed. A higher heating rate does not mean that the densification mechanism is modified, as shown by the applicability of the unifying Master Sintering Curve concept.[48] But in some cases (and possibly due to adsorbed water) higher heating rate can lead to higher final density, as shown for nanocrystalline zinc oxide and hydroxyapatite.[49,50] The fast densification by FAST/SPS can also reduce the interaction between the sintering material and graphite tool. An example is the full densification of boron suboxide (B_6O) showing very high-hardness values of up to 45 GPa achieved in graphite dies by FAST/SPS whereas the synthesis in HP requires expensive hexagonal BN dies.[51]

Additional thermal effects in FAST/SPS are related to high local temperature gradients or non-uniform temperature distribution as well as macroscopic temperature fields creating thermal stresses.[52] Temperature gradients in the sample can be evaluated by Finite-Element Modeling, as shown in Section 4. Microscopic temperature gradients provide an additional driving force for diffusion, which is known as Ludwig–Soret thermal diffusion or may even induce local melting. However, the build-up of such local thermal gradients strongly depends on the physical properties and size of the particles and grain boundaries.[53] It appears that for mixed or ionically conducting ceramics and grain size in the sub-micrometer or micrometer range possible local temperature gradients can be neglected. In addition Kuzmov *et al.*[54] estimated for aluminum grains smaller than 25 μm that local temperature differences between neck and center of the particles are less than 10 K.

2.3. Electrical Effects

The electrical effects can be differentiated into field and current effects and have been recently described in detail in two book chapters.[55,56]

If an electrically conducting raw powder is processed by FAST/SPS, high-electric currents flow directly through the green body rather than through the surrounding (graphite) tools. In that case, possible interactions between the electric current and the microstructure formation during sintering become relevant. These are: (i) percolation effects of the current in the initially porous powder bed,[57,58] (ii) the Peltier effect at the interface between green body and punches,[59] (iii) electrochemical reactions and the interfaces[60] and electromigration.[1]

Since the green body is not completely homogeneous and dense, the electric current cannot flow through the material homogeneously. Instead, a complicated network of percolating current paths will form, which is a consequence of the initial packing structure of the green body. The Joule heating, fundamental to the FAST/SPS process, occurs along the percolating current paths. Fluctuating hot spots form within the percolation network, characterized by high local current densities and (over) heating. The temperature within these hot spots can exceed the average temperature of the process considerably, leading to mechanisms of microstructure formation, which differ from standard sintering scenarios, like for instance partial melting and recrystallization. As a consequence of the inhomogeneous energy distribution within the sample, local temperature variations dominate the development of the microstructure. Within the current paths and even more dominant, within the hot spots, densification sets in much faster than in neighboring sample regions with lower current density. As a consequence of the on-going compaction, the conductivity of the material close to the current paths rises and the percolation pattern "burns into the microstructure. Fingerprints of this percolation pattern may then be found in the sintered product. This was demonstrated for SPS of silicon nanoparticles, where patterns related to the temperature fluctuations due to percolation effects were found on the length scale of micrometers.[58]

Another direct effect of the electric current flowing through the sample is due to the Peltier effect. Peltier heating or cooling occurs if an electric current I flows through a materials' interface due to the discontinuity of the Peltier coefficients Π of the two materials in contact, since the electrons carry a different amount of heat within the two materials, expressed by the specific Peltier coefficients. The heating or cooling $\dot{Q}$ delivered to the interface is

$$\dot{Q} = \Delta\Pi \cdot I$$

and therewith directly proportional to the current. Typically, high-current densities are used in FAST/SPS, in the order of a few kA cm^{-2}. If a metallic powder is processed, the difference of the Peltier coefficients between the green body and the electrodes (punches) is small and can mostly be neglected. The situation is different if a semiconducting powder is processed by FAST/SPS. Semiconductors have much higher Peltier coefficients than metals or graphite, resulting in considerable Peltier heating or cooling at the electrode/green body interface which can reach up to 10% of the total heating power delivered by the process.

In contrast to Joule heating, the Peltier effect depends on the direction of the current. For instance, the anode will be additionally heated if electrons are the majority charge carriers in the semiconductor. The anode will be cooled, if defect electrons (holes) are the majority charge carriers. Especially, if the temperature control is realized by a pyrometer close to the anode, the described Peltier effect biases the temperature measurement and process control

ADVANCED ENGINEERING MATERIALS

significantly. This anisotropic heat distribution could be avoided by applying an alternating current (AC) instead of a DC or by a precise matching of the Peltier coefficients of electrode and sample materials. Both of these possibilities are technologically challenging and currently not implemented in standard machinery.[59] Electrochemical reactions at the electrodes or electromigration are further direct effects of the electric current, which couple back into the development of a specific microstructure. Electrochemical reactions at the electrodes were successfully employed to demonstrate a novel crystal growth route toward an intermetallic clathrate, $Na_{24}Si_{136}$.[60] Starting from a suitable precursor, the silicide formation was realized by oxidation of Si_4^{4-} at the anode, while the sodium was reduced at the cathode. By this method an otherwise hardly accessible complicated cage structure could be synthesized due to the specific nature of the current activated sintering technique.

Evidence for electromigration in FAST/SPS is more difficult to find. When a current flows through a material, electrons scatter at the lattice atoms – especially if they are charged – and, by doing so, transfer part of their energy and momentum to the lattice. Due to the direction of the current, this scattering creates a preferred direction for the diffusion of the lattice ions. Integrated circuits are known to fail because of electromigration, but very high-current densities are typically necessary to trigger electromigration (up to several 100 kA cm^{-2}), which exceed the current densities usually employed in FAST/SPS. Besides, electromigration is a relatively slow process, and one of the major advantages of SPS/FAST is that the total sintering time is quite short, only in the range of several minutes to a few hours. Munir and co-workers performed several experiments in which they demonstrated the formation of intermetallic phases dramatically benefited from the electric current. While temperature alone did not induce the formation of intermetallic phases in a layered system of Al/Au or Si/Mo, an experimental set-up with a current flowing through the interfaces induced the formation of intermetallic phases. This effect depended on the current density, but not on the current direction.[1] Due to the evident dependence of electromigration on the current direction, the authors discuss several possible origins of their observations besides electromigration, like a change in defect concentration or enhanced mobility of defects due to the electric current. Electrochemical reactions at the materials interfaces, as discussed above, might be an additional option.

Electrical fields (without current flow) are known to affect matter transport, grain boundary migration, and possibly defect.[61,62] However, the voltages applied in FAST/SPS are very low, usually lower than those required to observe the above-mentioned effects. That's why for alumina or fully stabilized zirconia no difference with HP could be highlighted, if the same processing parameters had been used in the comparison experiments.[32,33] Nevertheless, for materials with high-dielectric permittivity, the electric field may be locally amplified by several orders of magnitude at interparticle junctions.[63] Further work is definitely needed in this area.

2.4. Role of Atmosphere

Usually, the composition of the sintering atmosphere and the partial pressure of its constituents have an influence on the defect structure and diffusivity in the sintering material. Therefore, densification kinetics,[64–66] grain growth,[67–71] phase stability,[72] oxidation number or stoichiometry[73–76] are affected by the sintering atmosphere. In general, the reduction in surface energy of the particles resulting from the adsorption of specific species of gas, water, or organics should be considered,[77] because this modifies the thermodynamical driving force to surface reduction and sintering. Schwarz *et al.*[49] observed not only an increased densification rate for nanocrystalline zinc oxide with moisture in FAST/SPS but also a remarkable difference in final density at a lowered sintering temperature. The presence of water vapor in the sintering atmosphere is known to enhance surface diffusion of magnesia doped alumina,[65] titania,[78] magnesia,[79–82] or zinc oxide[64] due to chemical interaction of water with the surface of the oxide and surface diffusion of hydroxyl ions and protons. A decrease in densification was observed when sintering in a carbon oxide atmosphere because of the formation of carbonate layers inhibiting diffusion.[64] Moreover, gases entrapped in closed pores are detrimental to achieve full density and can even lead to desintering due to pressure build-up.[83] Coble showed for MgO-doped alumina that nearly full densification could be achieved by sintering in either hydrogen or oxygen but not in helium, nitrogen, or argon.[84] These latter gases have a low solubility and diffusivity in alumina and can therefore not be eliminated from residual pores. Kang and Yoon[85] assumed that densification with gas pressure is ending at the point where the pressure inside a pore P_f is $P_f = 2\gamma/r$, whereat γ is the surface tension and r is the radius of curvature at the pore surface.

By decreasing gas pressure in the sintering chamber, surface contamination of the powder particles is decreased. Vacuum is further used to avoid the reaction with nitrogen, hydrogen, or oxygen especially for metallic materials.[86] It is often estimated that desorption takes place with increasing temperature but it should be noted that, e.g., for some metals adsorption of hydrogen increases with raising temperature. The evaporation of the sintering material itself as described by the Langmuir equation can lead to a change in composition/stoichiometry and/or formation of defects.[86]

To summarize, atmospheres present in FAST/SPS are typically low vacuum (in the range of 10^{-4} to 10^{-5} bar), [87,88] inert gas (i.e., argon or nitrogen, up to 1.3 bar) or reducing hydrogen gas mixture (i.e., forming gas), which are recommended atmospheres for sintering metals and non-oxide ceramics. However, as the sample is enclosed in the pressing tool, pressure and composition inside the tool can strongly differ from the atmosphere outside. A rapid desorption of gas (e.g., TiH_2 decomposition) during the fast heating can even create gas pressures, which can destroy the die. Therefore, hardly any information about the real gas composition and

pressure in the sample is given in most of the literature. As standard graphite tool starts to react at temperatures above 600 °C with oxygen present in the sample itself, oxygen partial pressure continuously decreases within the furnace and especially in the pressing tool. The formation of CO due to reaction of adsorbed moisture, oxygen, or reaction of oxides in the material with the graphite die results in a reducing atmosphere and intensive gas phase transport can take place between the sample and the die as long as open porosity exists. This can result in reduction of oxides or even precipitation of carbides and carbon in the sample.

Consequences of the reducing atmosphere are numerous for oxide materials. Recnik *et al.*[76] showed for $BaTiO_3$ that an increased concentration of oxygen vacancies due to the reducing atmosphere could lead to a lower density of ferroelectric domains. An *et al.* found out that for TiO_2 doped $BaTiO_3$ no abnormal grain growth or twin formation occurred when samples were sintered in highly reducing atmosphere (hydrogen) in contrast to samples sintered in air. They explained the absence of abnormal grain growth by an increase in the concentration of ionic vacancies and thus reducing the critical driving force for grain growth.[71] Moreover Jiang and Mukherjee[89] showed that optical transmission of yttria-magnesia composite samples was degraded by changing the annealing atmosphere from air (ambient atmosphere) to vacuum (in FAST/SPS). The decrease in transmission after sintering or annealing in FAST/SPS was attributed to an increase in the concentration of oxygen vacancies, which act as color centers and darken the specimens (see also Part 3.3). Thermoelectric perovskite material $Ca_{0.9}Yb_{0.1}MnO_{(3-x)}$ sintered by FAST/SPS in vacuum showed significant oxygen deficiency ($x = 0.21$) detrimental to its properties compared to samples sintered in atmospheric FAST/SPS ($x = 0$–0.03).[75] The use of alternative carbon-free pressing tools might be a new way to address such issues and guarantee the optimal sintering atmosphere for each material.

3. Materials Development

3.1. Refractory Metals and Intermetallics

Refractory metals such as W, Re, Os, Ta, Mo, Nb, Ir, Ru, and Hf have melting points higher than 2000 °C, good thermomechanical properties, creep and wear resistances at high temperature, outstanding electrical and thermal conductivity.[90] Among them, tungsten and its alloys is the most used material due to its highest melting point (3683 K), high strength, low coefficient of thermal expansion, and excellent thermal and electrical properties.[91] Refractory metals require high temperatures for their densification and reducing atmospheres or vacuum during the sintering process due to their tendency to oxidize. Full densification can only be achieved using external pressure, thus hot isostatic pressing (HIP), HP with induction heating, and FAST/SPS are the most common techniques for the densification process.[86] Nevertheless, full densification of these materials with final nano/sub-micron grain size still remains a challenge. In addition, oxygen contamination of the powder hinders the diffusion-driven mass transport during the sintering process. Oxygen impurity content increases as the particle size is reduced. FAST/SPS usually enables a better control of the final microstructure, thanks to high-heating rates and short dwell times at the maximal temperature. As discussed in Part 2, FAST/SPS can enhance densification in comparison with others techniques by primarily two effects: (i) current flow through the specimen – provided that the interparticle contact resistances are not too high-enhancing diffusion processes and (ii) local vaporization or melting of the powder surface as well as elimination of the oxide surface layer due to higher local temperature at the sintering neck.

Initial particle size plays a critical role in the densification process of pure tungsten. Green bodies made out of particles larger than 10 μm present little densification nor grain growth when sintered freely at 2500 °C, while starting particle size smaller than 2 μm can be densified at 2000 °C nonetheless accompanied by a 10-fold increase in grain size.[86] Use of FAST/SPS with similar starting grain size leads to a dramatic reduction of the maximal temperature (1300 °C) necessary for densification of tungsten with negligible grain growth.[92] If full densification is required, higher temperatures inducing exaggerated grain growth are needed or FAST/SPS must be combined with other techniques including ultrahigh pressure.[93] Tungsten heavy alloys (WHAs), such as W–Fe–Ni, are commonly densified by liquid phase sintering at temperatures above 1460 °C, where the final composites present large tungsten grains, typically 30–40 μm in size. FAST/SPS enables a better control of the microstructure and a reduction of the final grain size.[94] During the initial stage of sintering in FAST/SPS, particle rearrangement and neck formation take place.[95] In the intermediate stage, tungsten grain boundary diffusion is enhanced by the presence of nickel during solid state sintering and, when a liquid phase is formed, the dissolution–precipitation of W grains in the viscous matrix is the dominant mechanism.

Refractory metals, i.e., tantalum,[96] molybdenum,[97] ruthenium,[98] and their alloys present similar densification behavior as tungsten:[86] negligible or limited grain growth below relative densities of ≈90–95% and exaggerated grain growth with scarce enhancement of the final density with further temperature increment. Comparison of pure ruthenium sintered by FAST/SPS and HP reveals a reduction of the residual stress when FAST/SPS is used.[98] This effect is correlated with an increased grain growth (37–42 and 29–36 nm for FAST/SPS and HP, respectively). Nevertheless, the heating rate and the maximal temperature are different for the two sintering techniques, thus further investigations are required to clarify the origin of the advantages provided by FAST/SPS for refractory materials.

Intermetallic materials are excellent candidates for high-temperature applications due to their intermediate properties between superalloys and ceramics, as they can present higher melting points than superalloys and better toughness

ADVANCED ENGINEERING MATERIALS

than ceramics. Nickel and iron aluminides are the most investigated compounds for high-temperature applications,[99] although Nb/Al and Ti/Al also show interesting thermomechanical response.[100] Processing of intermetallic materials commonly involves a prior mixing process of the basis metals by mechanical activation to form a solid solution followed by the consolidation of the obtained intermetallic compound by sintering. FAST/SPS leads to the full densification of the specimens with a finer microstructure in comparison with conventional techniques,[101] allowing dense materials with grains in the nano-scale range, as shown for Ni_3Al,[102,103] FeAl,[104,105] and TiAl.[106–108] More examples of sintered intermetallic materials are reviewed by Orru *et al.*[109] In order to increase the creep resistance at high temperature, second oxides phases are frequently added or formed in situ by mechanical alloying (oxide-dispersion-strengthening (ODS)).[110] These particles act as rigid inclusions – against the densification of the composite material – but also pinning the grain boundaries and lowering their mobilities according to the Zener model. On the other hand, their incorporation may help the densification process by local liquid phase sintering mechanism as it is the case with Y_2O_3.[111] Alternatively, the electric field may enhance the precipitation rate of complex (Y, Al, and Fe) oxides from supersaturated solid solution.[112]

3.2. Ultra-High-Temperature Ceramics (UHTC)

UHTC materials are borides, carbides, and nitrides of the Group IV–V elements of the periodic table (Zr, Ti, Hf, and Ta), which present the peculiarity of melting temperatures in excess of 3000 °C. Besides high-melting point they also exhibit high electrical and thermal conductivities, high refractoriness, chemical inertness against molten metals, outstanding thermal shock resistance, and excellent mechanical response in a wide range of temperatures.[113] Due to the unique combination of mechanical and physical properties potential applications of UHTC are related with components that work under extreme temperatures conditions, such as thermal protective structures for leading edges on hypersonic flights and during atmosphere exit and re-entry processes on aerospace vehicles, aero propulsion systems, refractory crucibles, and plasma-arc electrodes.[114,115] ZrB_2 and HfB_2 are the most studied and employed UHTC materials,[116,117] although TiB_2,[118] ZrC,[119] TaC,[120], and TiN[121] also show interesting properties.

Sinterability of UHTC materials is low due to the high-covalent character of atomic bonding, low self-diffusion coefficients, oxygen impurities located on the particle surfaces and the micrometer size of commercial powders. These intrinsic and extrinsic characteristics entail high temperature and pressure for densification. HP have been historically used for the sintering process, although rapid grain growth at high temperatures entrapped residual pores.[116] In that sense, FAST/SPS technique is an excellent solution to densify UHTC ceramics due to the combination of uniaxial pressure, high-heating rates, and short sintering times at the maximal temperatures, which allows the control of the final microstructure. Nevertheless, enhancement of the sinterability by refining the starting powder and removal of oxygen impurities is still desired.

Refining the starting powder is a common process in ceramic processing for increasing the densification rate. Thompson *et al.*[122] studied the densification of ZrB_2 with different particle sizes, $\approx 2\,\mu m$ for as-received powder and $\approx 0.2\,\mu m$ obtained by attrition milling. This reduction in particle size increased the final relative density from 70 to 97%, respectively, maintaining the same sintering conditions. Improvements in sintering kinetics and final densities are even higher if the crystal size is reduced to the nanoscale, as was reported by Zamora *et al.*[123] Fully dense material was obtained when the particle size was reduced down to $\approx 10\,nm$. Nevertheless, exaggerated grain coarsening may take place at the high temperature required for densification (above 1900 °C).

As for metals, contamination by oxygen is detrimental to densification because it hinders diffusion-driven mass-transport mechanisms during consolidation of UHTC. As shown in TaC, oxygen impurities present in the starting powder may also favor exaggerated grain growth if evaporation–condensation mechanisms become active at high temperature.[124] Reduction of oxygen by C or B_4C additives therefore enhances the densification process of TaC.[125] Oxygen removal is also possible by adding $MoSi_2$, $TaSi_2$, or SiC.[126,127] $MoSi_2$ reacts with surface oxides present on HfB_2 particles, forming silica and liquid Mo–Si–B alloys at high temperature. The use of additives also improves the mechanical properties and the resistance to oxidation at high temperature that are critical factors for the final applications of UHTC materials.[128,129]

Despite the reduction of the sintering temperatures and the better control of the final microstructure provided by FAST/SPS, the existence of specific mechanisms present in FAST/SPS in comparison with other techniques has not been cleared out yet. At least one property of UHTC to consider is the high electrical conductivity ($\approx 10^7\,S\,m^{-1}$ at room temperature, more than 2 orders of magnitude in comparison with the graphite used for pressing tools). Current is thus supposed to flow through the specimen, possibly enhancing diffusion processes as detailed in Part 2. However, in-depth investigations are required. Mizuguchi *et al.*[130] compared by transmission electron microscopy ZrB_2 samples sintered by HP and FAST/SPS. Lower impurities at grain boundaries were observed for the FAST/SPS samples, effect which was attributed to the cleaning of particle surfaces due to electrical discharges generated between particles.

3.3. Transparent Ceramics

Polycrystalline transparent ceramics potentially present several advantages compared to single crystals: easier shaping, larger dimensions, better mechanical properties

(hardness, wear resistance, and fracture strength), higher resistance against thermal shock, flexibility in terms of chemical composition and doping, lower processing temperature, and reduced production costs. Possible applications of transparent ceramics include solid state lasers, lenses, wavelength converters for LED lighting, scintillators, arc discharge tubes, windows for infrared detection and thermography, transparent armors, or protective windows for watches, jewels, etc.[131]

The development of such advanced materials has recently raised a large interest in the research community. Fine microstructure including the removal of possible sources of light scattering (inclusions, second phases, and porosity) is challenging. Transparency further depends on the wavelength considered: the real in-line transmission is usually closer to the theoretical one in the infrared range than for shorter wavelengths (including visible light). As pore size is usually in relation with grain size, a smaller grain size is almost always advantageous.

Transparent ceramics synthesized by FAST/SPS include a large number of optically isotropic materials[132] like yttrium-aluminum-garnet (YAG), pure or doped with rare earths,[133–136] yttria,[137] magnesia,[138] magnesium aluminum spinel,[139,140] fully stabilized zirconia,[141] and lutetium based oxides.[142] Optically anisotropic ceramics are even more challenging, as the transparency decreases drastically as grain size increases, and alumina,[143–146] tetragonal zirconia,[147] or hydroxyapatite[148] have been synthesized with improving success.

Compared to standard free sintering in vacuum followed by HIP, the definite advantages of FAST/SPS are: (i) one single set-up required for densification and (ii) shortening of the process cycle. Nevertheless, initial powder quality and homogeneous packing are crucial to obtain transparency.[131] By first manufacturing agglomerate-free green compacts by slip casting or pressure filtration, larger pores detrimental to light transmission can be removed.[149] Doping, mixing with additive forming a transient liquid phase such as LiF are further means to improve densification and transparency.[134,145] Empirical approach is generally used to finely tune the process parameters and gain a maximized transparency. Typically, a first rapid heating step up to an intermediate temperature is followed by a slow ramp (below 10 K min^{-1}) to the maximal temperature in order to get rid off the last pores.[139] Compromise between required pore closure and undesirable grain growth determines the holding time at elevated temperature. In some cases, no holding time at all might be necessary. When using intermediate pressures and standard graphite tools, a two-step pressure schedule might be advantageous to homogenize the microstructure.[144,150] However, possible contamination by carbon at least at the contact surface with graphite parts[151] and the creation of light-absorbing oxygen vacancies due to reducing conditions[152] both lower the in-line transmission. Usually, a post-sintering annealing step in air improves the transparency. Another approach relies on the application of high pressure, as described in Part 2.1.[42,145] Application of high pressure removes heterogeneities in the microstructure while achieving near theoretical density.

3.4. Nanostructured Materials

Nanostructured materials are desirable either because of their superior mechanical properties, wear resistance[153] or because of improved functional properties like thermal or electrical conductivity[154] as compared to their microcrystalline counterparts. The nanometric crystallite size directly affects the thermodynamic equilibrium phase of polymorphic materials as for instance zirconia, alumina, or titania. Functional properties like thermal or electrical conductivity, dielectric, piezoelectric, and ferroelectric properties, magnetic properties or optical transparency (Section 3.3) can be directly tuned by the nanometric grain structure.[154] For this, it is necessary to achieve an average crystallite size well below 50 nm, often below 10 nm, in the densely compacted bulk material. This can be obtained by FAST/SPS, starting with a nanocrystalline raw powder, even in the absence of electrical effects. Short heating times and the applied pressure (see also Section 2) result in an enhanced rearrangement and partial destruction of agglomerates. The early stages of densification of nanopowder compacts proceed either by the plastic deformation of particles, grain rotation, and sliding, aided by softening of the particle surfaces.[37,130] These processes allow fast densification with limited grain growth. In some cases, grain coarsening may be further reduced by optimizing the temperature schedule. A rapid densification step followed by a low temperature hold (known as two step sintering)[155] achieves as in free sintering but in much shorter time a last gain in densification with very limited grain growth.[156] Also, the application of modified rate controlled sintering schedules may be beneficial for the densification of nanopowders.[157] A detailed overview over the preparation and properties of nanocrystalline functional ceramic materials is given by Maglia *et al.*[154] and Chaim *et al.*[158]

A high-pressure FAST/SPS process was used to sinter pure zirconia, size-stabilized in the tetragonal polymorph, with a relative density above 90% and an average grain size well below 50 nm[154,159] as well as to sinter titania, size-stabilized in the tetragonal polymorph (anatase).[160] Nanostructured bulk $BaTiO_3$ with a relative density above 97% crystallizes in the ferroelectric tetragonal equilibrium phase, but with a reduced tetragonal distortion as compared to the polycrystalline bulk.[161] This finding holds for nanostructured $BaTiO_3$ samples with a grain size of 20 nm and a relative density of 97% as shown by Deng *et al.*[162] Note that nanostructured bulk $BaTiO_3$ and $SrTiO_3$ were also prepared with a high-optical transparency, with transmittance of up to 90% in the visible and near infrared regions.[163] In ferroelectric mixed ceramics of the $BiScO_3$–$PbTiO_3$ system, nanostructured bulk samples with an average crystallite size down to 30 nm were characterized with respect to their relative permittivity.[164]

ADVANCED ENGINEERING MATERIALS

There were indications that the ferroelectric phase transition of this ceramic material (i.e., monoclinic distortion) vanishes for the smallest grain size of 30 nm. Analogously, in the mixed relaxor ceramic $Pb(Zn,Nb)O_3$–$PbTiO_3$ system, the ferroelectric to relaxor transition disappears for small crystallite sizes of 20 nm.[165] Magnetic nanostructured bulk cobalt–iron spinel, $CoFe_2O_4$, was successfully fabricated by Imine *et al.*[166] with an average crystallite size of only 11 nm and a relative density of >92%, and superparamagnetic behavior was demonstrated for those samples. Magnetic nanostructured bulk Ni–Zn ferrites were synthesized by Valenzuela *et al.*[167] Their samples had a relative density between 92 and 94% and an average crystallite size around 60 nm. The authors showed a random distribution of the anisotropy axis and concluded that the crystalline grains were single magnetic domains.

An important upcoming field of application for nanocrystalline materials processed by FAST/SPS are thermoelectric generators, which directly convert heat fluxes into useable electrical energy. Such generators are expected to be used for miniaturized autarkic sensors, heating systems, and waste heat recovery, e.g., in automotives or general combustion machines, and on the long term perspective waste heat recovery for medium-scale industrial facilities.[168] Thermoelectric materials are (compound-) semiconductors, which combine a unique combination of transport properties such as a high Seebeck coefficient, a high-electrical conductivity but a low-thermal conductivity. This combination is rare since typically materials, which are good electrical conductors also conduct heat very well. The transition to nanostructured materials is therefore a means to improve the efficiency of a thermoelectric material, since the nanostructure reduces the thermal conductivity of the material dramatically while maintaining the electrical transport properties. Consequently, FAST/SPS has become meanwhile a method of choice to improve the thermoelectric efficiency of many materials.

FAST/SPS was applied to sinter dense thermoelectric materials 15 years ago by Japanese groups[169,170] using microcrystalline raw powder. One main idea was to reduce the manufacturing costs by applying a rapid sintering technique[169] to process thermoelectric oxides like $Ca_{2.75}Gd_{0.25}Co_4O_9$[171] or $Ca_3Co_4O_9$.[172] These oxide samples had a density of more than 96% resp. 99% of the single crystalline material. The samples were compared to a conventional sintering method within a furnace, which resulted in much lower density material (66%) and to hot pressed material. The FAST/SPS processed samples showed significantly improved properties due to a very high-electrical conductivity and therewith electrical power factors as a result of the high density.

One of the first nanostructured thermoelectric bulk materials processed by "DC hot pressing" was presented by Poudel *et al.*[173] Using this combination of ball milling and FAST/SPS, they showed that the thermoelectric conversion efficiency of a BiSbTe alloy was approximately 40% higher for the nanostructured "DC-hot-pressed" material compared to the microcrystalline reference sample. Also, other thermoelectric materials like SiGe alloys[174,175] or silicon[176] showed great improvement due to the application of FAST/SPS. Also nanostructured bulk oxides like Ga-doped ZnO,[177,178] TiO_2,[179] or $SiTiO_3$[180] were characterized with respect to their thermoelectric properties and generally show a reduction in thermal conductivity when compared to their polycrystalline reference. A further development is the combination of mechanical alloying and FAST/SPS to produce nanostructured or fine grained compound materials as shown for $AgPb_mSbTe_{2+m}$ [181] Hierarchical nano- and microstructured composite materials fabricated by FAST/SPS exhibit current record values in the thermoelectric efficiency.[182] Tabulated data on selected nanostructured thermoelectric compounds can be found in ref.[168]

However, as stated by Maglia *et al.*,[154] an evaluation of the long-term stability of the functional nanostructured materials has rarely been done and needs to be addressed for future applications.

3.5. Functionally Graded Materials (FGM)

FGMs present a gradient of composition, grain size, or porosity in 1, 2, or 3 dimensions. Although the concept of gradient materials was already published in 1972,[183] interest from industry and research community only raised in the mid-1980s. Innumerable applications in mechanical engineering, biomaterials, nanotechnology, electrical, and thermal systems are based on the local variation of properties within the material.[184,185]

From a processing point of view, gradients can originate from the powder and green body itself or may be induced during sintering. Numerous methods, such as powder stacking, sheet lamination, slip casting, wet powder spraying, centrifugal deposition, pressure filtration, or gravity sedimentation have been used to fabricate layered or continuously graded green compacts. However, inhomogeneous powder properties lead to severe cracking problems during free sintering. Superposition of an external pressure helps to solve this problem, and HP, HIP, and FAST/SPS are required for the complete densification of FGMs. For instance, laminated TiN/Al_2O_3 and layers of $(TiN)_x(Al_2O_3)_{1-x}$ (x ranging from 1 to 0), [186] hydroxyapatite/yttria stabilized tetragonal zirconia,[187] ZrB_2/ZrO_2,[188] $Ti/TiB_2/B$,[189] Ni/Cu,[190] mullite/molybdenum,[191] ZrO_2/stainless steel,[192] or Al_2O_3/SiC[193] were successfully densified by FAST/SPS.

On the other hand, FAST/SPS opens new possibilities for the development of FGMs, based on the generation of a temperature gradient during sintering. This is enabled through the modification of the heating elements. As thermal energy is produced by Joule heating in the die and punches, a variation of cross-section in the conducting tool will produce a temperature gradient. A smaller cross-section locally increases the current density and consequently the temperature. Asymmetric systems (Figure 3b and c) allow obtaining FGMs in one step from an initial homogeneous powder compact, reducing the number of manufacturing processes

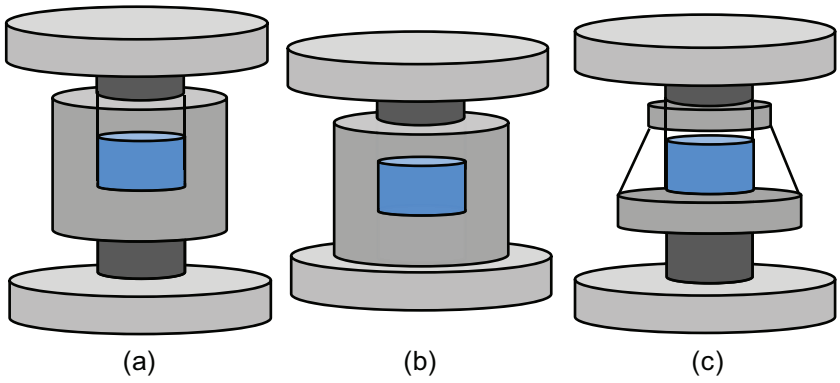

Fig. 3. (a) Symmetric configuration of the heating elements, (b) asymmetric location of the graphite die, and (c) asymmetric graphite die.

and saving time and costs. The development of a continuous gradient is also beneficial from the point of stress distribution, avoiding stepped stress profiles, which may lead to delamination.

Dense specimens of silicon nitride with a continuous gradient in phase composition and grain size were obtained by Belmonte *et al.*[194] using the asymmetric configuration of the graphite components (Figure 3b). In just 4 mm distance, the α phase content could be continuously varied from 6 to 85% (at 1550 °C) and the grain size ranged from 500 to 200 nm (at 1650 °C). Another alternative for the modification of the temperature profile is to use an asymmetric graphite die, as shown in Figure 3c. The first mention of this die geometry in 2008 by Hong *et al.*[195] was to counteract the effect of a gradient in composition of a $ZrB_2/SiC/ZrO_2$ composite. Recently, Liu and Jin[196] obtained continuous FGM based on TiAlN/TiN through the reaction between Ti and AlN from a sole initial composition. Difference of temperature between top and bottom can be of several hundreds of degree celsius, as shown for TiB-Ti specimens.[197] Finally, an increase in the heating rate can also lead to a large axial (and not only radial) temperature gradient.[198] Such temperature distribution can be predicted by modeling software as presented in Section 4.4.

3.6. Non-Equilibrium Materials

Non-equilibrium materials are a group of materials that cannot be produced by conventional sintering methods like free sintering or even HP since they react or transform into a new phase due to their metastability at atmospheric pressure and/or high temperature. Short sintering cycle and exposure time to high temperature as well as high pressure applied in FAST/SPS enable the consolidation of such materials in their metastable state due to kinetic reasons. Such non-equilibrium materials can show new interesting combination of mechanical, electrical, and thermal properties. Therefore, new multifunctional and hybrid material concepts with a wider range of properties can be obtained by FAST/SPS. The following examples of such materials will demonstrate the potential of this approach.

FAST/SPS allows to produce ZrO_2/apatite composites, as the fast sintering prevents the interaction of the components and the decomposition of hydroxyapatite. The resulting material is a high-strength bioactive material, which offers new possibilities for biomedical applications.[199] Also, non-equilibrium dielectric and piezoelectric materials can be produced by mixing perovskite powders of different compositions. As full densification is achieved by FAST/SPS without complete interdiffusion of the cations, the final properties result from the superposition of the properties of the original perovskites. This allows tuning the temperature coefficient of dielectric properties over a wide range of values.[199] Even for more traditional materials like silicon nitride and SiAlON, new combination of properties can be achieved. α-Silicon nitride powders used for the production of ceramics transform into a high temperature β-phase by a dissolution–precipitation mechanism showing grain growth of the β silicon nitride. By FAST/SPS, the content of α and β phase can be adjusted in one sintered specimen, which leads to an increase in hardness (α-phase) and fracture toughness (β-phase), [200,201] improvement of the wear resistance and reduction of the friction coefficients as well as longer life time in ball bearings.[202] On the other hand, the applied pressure and the addition of seeds can be used to prepare strongly textured or extremely fine-grained piezoceramics, resulting in strong anisotropic properties interesting for sensor and actor applications.[203]

Supersaturated solid solutions of aluminium alloys, which could not be produced by casting can be densified by FAST/SPS. The mechanical properties of such non-equilibrium aluminum alloys are however lower in comparison to wrought or extruded compacts due to the oxide layers initially present on the surface of the particles. Additional hot extrusion destroys at least partially these oxide films and strongly increases the strength of the materials.[204] Zhang *et al.* has focused their attention on high cooling rates to produce metastable Ti–Al–V alloys with high ductility. A similar approach can be used for many other systems. The high-cooling rates can result in special microstructures or special non-equilibrium phase assembly.[205]

Further examples of non-equilibrium composites are diamond or cubic boron nitride containing materials. The hard reinforcing phase secure good tribological properties as well as high hardness.[206] A wide range of cBN or diamond-based composite materials with ceramic or hard metal matrix has been successfully produced by FAST/SPS.[207–214] Pure carbon nanotubes (CNT) can be densified with FAST/SPS without decomposition up to a density of 1.29 g cm^{-3}. The remaining pores are all below 6 nm.[215] Also, the densification

ADVANCED ENGINEERING MATERIALS

of CNT/ceramic composites was investigated intensively showing the possibility of full densification with minimal decomposition of the CNTs and achieving special electrical and wear properties.[216–223] The structure and quality of the interfaces between organic and inorganic constituents plays a decisive role for the final properties of the composites.

The formation of diamond from fullerene C60 without any catalysts was also possible in FAST/SPS run under moderate pressure of 50–80 MPa at 1150–1300 °C with a heating rate of 100 °C min^{-1} in vacuum, i.e., much "milder" conditions than usually required for diamond production.[224,225] Polycrystalline diamond crystals with sizes up to 250 μm and transition rates about 30% were observed. The transformation into diamond takes place by direct reconstruction of sp^3 carbon, which exists as a high fraction in the fullerene. As shown by these few examples, the development of non-equilibrium materials via FAST/SPS is only in its infancy. A wide range of new materials and applications can be expected in the near future.

4. Technological Development

4.1. New Concepts for FAST/SPS Devices

Latest developments have led to a change from small lab-scale devices for batch production to larger furnaces suitable for industrial production. One main aspect is the reduction of total cycle time, especially cooling to room temperature, which is the most time intensive step for large samples. Productivity of a large-scale FAST/SPS plant can be doubled if a separate cooling chamber is installed. After sintering the hot tool is automatically transferred to a second chamber in which the cooling takes place whereas a new run can be started in the FAST/SPS chamber.[226,227]

Another increase in productivity can be achieved by fully automating the FAST/SPS process. Automated tool assembly, powder filling, pre-heating, consolidation, and cooling in a separate chamber was first reported in 1999 for the production of steel–zirconia FGMs.[228] Since the size of such a plant is very large, another possibility to increase the productivity for small products is dry pressing technique combined with FAST/SPS consolidation.[226,229] In that case, a suitable tool is automatically filled with powder and the powder is uniaxially compacted before a direct electrical current is applied to heat up the powder compact. After sintering to complete density, the hot product is ejected and new powder is filled into the cavity. Such a "FAST" system is being developed at the moment within the SeProFAST project to efficiently produce near-net-shaped products (for instance facetted cutting tool inserts) with a cycle time below 1 min.

The establishment of a homogeneous temperature distribution within very large parts is another challenging task. Largest FAST/SPS apparatuses allow diameters of sintered parts up to 400 mm. The design of suitable tools must be provided by finite element calculations. It could be shown that the application of an additional induction or resistance heating source surrounding the die leads to a more homogeneous radial temperature distribution[226] compared to sole FAST/SPS heating. In hybrid systems, direct Joule heating and induction heating can be independently controlled. Such concepts have been actually known since 1938 for a combination of direct electrical and resistance heating[230] and since 1965 for direct electrical and induction heating.[231] Finally, when sintering magnetic powders, superimposed pulsed magnetic excitation seems to improve temperature homogeneity by skin effect and better densification due to the Lorentz force acting on particles.[232]

4.2. Near Net Shape Processing and New Tool Concepts

The driving force in tool development is to allow the flexible production of more complex or near-net-shape parts and to raise the productivity by sintering larger or multiple parts in one cycle. Finishing costs and the loss of raw material by means of sawing and grinding can then be minimized.

The production of near net shaped products by means of FAST/SPS is not an easy task. A few examples are known from literature.[227,233] The main challenge is the construction of a suitable tool, which provides a uniform temperature distribution during heating and dwell time. Especially, sharp edges of such near-net-shaped tools act as heat sinks since heat losses are more dominant in those regions. Beside this idea, the concept of Spark Plasma Extrusion (SPE) was introduced by Morsi *et al.*[234] He describes a tool with two separated cavities. In the first cavity, the powder is getting heated and afterwards squeezed into a second cavity, which has a more complex geometry. Densification is enhanced since the squeezing into the second cavity additionally involves shear force. FAST/SPS can also be used as hot forging device, if the densified material present good superplastic behavior.[235,236]

Figure 4 shows examples of tool designs to increase productivity for industrial applications by parallel, serial, or parallel-serial alignment of tool cavities.[226,233] The tool design depends on the parts diameter and height and the usable room between the pressing rams of the furnace.

Since FAST/SPS uses a uniaxial pressing motion, the product shape is limited to simple shapes without undercuts. Flat or slightly bent, round, or polyhedrical geometries with openings have been proven feasible. Taylor[237,238] showed a drawing of a serial aligned tool for the production of bonded diamond articles already in 1933. Other examples were published by Schmidt *et al.*[239,240] or Tokita,[241] including alumina nozzles with a tapered outer diameter or aspheric glass lens molds made out of nano-WC.

Finally, new suitable tool materials may be required depending on the application.[226,242] Graphite, which is used in most cases in literature (typical specific electric resistivity 15 μΩ m, compressive strength 100–150 MPa) can be reinforced with carbon fibers to increase its mechanical strength.[43] For sintering temperatures below 1000 °C, steel

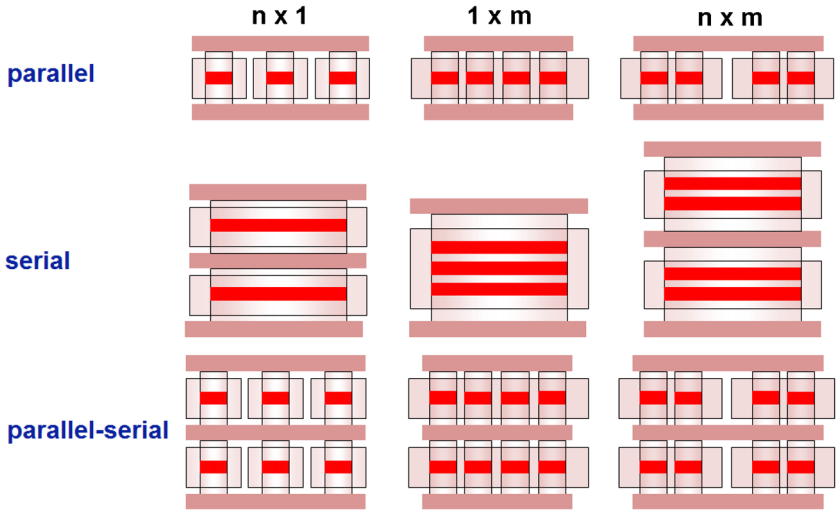

Fig. 4. Overview of tools for the production of multiple parts.

and refractory metals such as TZM molybdenum alloys, copper-beryllium, alumina,[243] silica,[244] and even concrete[245] were used. Anselmi-Tamburini *et al.*[141] used binder-free tungsten carbide parts with silicon carbide inserts. Double-walled tool concept with inner ceramic die and outer graphite mantle has also been proposed.[246] The choice is much more limited for temperatures above 1500 °C. Because of their outstanding mechanical properties at high temperature, bulk hexagonal boron nitride, boron carbide, titanium nitride, and carbide, as well as composite materials might offer interesting application perspectives. Also, layers and foils out of alumina,[32] hexagonal boron nitride,[247] and different metals (molybdenum, tungsten, and tantalum) can be used to separate graphite parts from the sintered compact, especially if they tend to react with each other.

4.3. Temperature Measurement and Control

The control of temperature in FAST/SPS, with heating rates of several hundreds of °C min^{-1}, is an important and critical matter. Main requirements for a reliable temperature measurement are a short reaction time, low lag, and a high reproducibility. Another aim is to measure as close to the sintering specimen as possible. This leads to the necessity of using different measurement methods for different types of applications.

The temperature is commonly measured by thermocouple placed in a radial hole inside the die or with a radial pyrometer focusing on the outside of the die (as typically installed in set-ups manufactured by Sumitomo Coal Mining Ltd., SPS Syntex Ltd.) or with an axial pyrometer measuring the temperature above the sample center (FCT Systeme GmbH). The measurement methods as detailed in Table 1 can be distinguished between optical and non-optical (contact) temperature acquisition, both having their own range of operation and limitations. Optical pyrometers are often used for high-temperature applications; however they cannot measure temperatures near room temperature. Depending on their specifications, the minimal temperature may be as high as 600 °C. They require that the focused surface has to be clean, the measuring channel needs to be free of obstructions and the emissivity ϵ of the die material needs to be known. However, non-optical temperature recording devices like thermocouples (TC) are able to measure from room temperature and show advantages in the positioning. Since, the thermocouple needs to contact the measuring-point, reactions between the tool material and the TC-casing need to be considered.

Temperature values reported in literature cannot be used in most cases directly to reproduce those experiments on other FAST/SPS devices,[248] especially if crucial details on tool configuration and dimensions are missing. When giving the sintering temperature it is important to detail the measurement method used as well as the measuring position. Large differences are commonly found between thermocouple and pyrometer measurements or between the temperature measured inside the tool and on the outer surface of the pressing die. By using the phase transformation from duplex $\alpha+\gamma$- to lamellar α-structure in $Ti_{48}Al_{48}Cr_2Nb_2$ to track the true temperature in the sample, Voisin *et al.*[249] showed that the radial pyrometer underestimated the temperature by

Table 1. Examples of optical and non-optical temperature measurement methods used in FAST/SPS.

Type	Position	Temperature range	Remarks
External optical pyrometer	**Axial**, inside pressing punch	250/600–3000 °C	Measuring very close to the sintering material, not suitable for very small diameters
External optical pyrometer	**Radial**, outer surface of die	250/600–3000 °C	Thermal insulation needs to be removed around measuring point
TC Type K (Ni-CrNi) with SS casing	No limit	RT–1100 °C	Bendable, tool material might react with casing, relatively cheap
TC Type C (W5Re-W26Re) with Mo-casing	No limit	RT–2200 °C	Limited bending, tool material might react with casing, expensive

ADVANCED ENGINEERING MATERIALS

50 °C compared to the axial pyrometer. Even more critical, Si_3N_4 was densified under the same conditions in two different set-ups using the same dies and same nominal time-temperature cycle. For monitoring the temperature conversion of the metastable α-Si_3N_4 phase into the β-Si_3N_4-modification was used. Differences in temperature of more than 200 K were observed under the same nominal conditions for a sample with a diameter of 20 mm.[250] This is due to the face that temperature was measured at different positions. Furthermore, Munir *et al.*[251] found temperature differences of over 150 °C when heating up an alumina sample at 200 °C min^{-1} up to 1350 °C and reading the temperature with a thermocouple inside the material and an optical pyrometer on the outer diameter of the die. Wang and Fu[252] even measured temperature gradients of up to 450 °C inside a 40 mm large TiB_2 + BN sample during heating at 170 °C min^{-1}. This indicates how important the clear description of the sintering setup is for the interpretation and comparison of results. The value and the direction of the temperature gradient in the sample and the die strongly depend on the conductivities of the densifying materials. For conducting materials, the surface of the die has usually a lower temperature than the samples. For insulating materials, usually the opposite situation is observed. Finite-element modeling enables to visualize such temperature gradients (as presented in Figure 5).

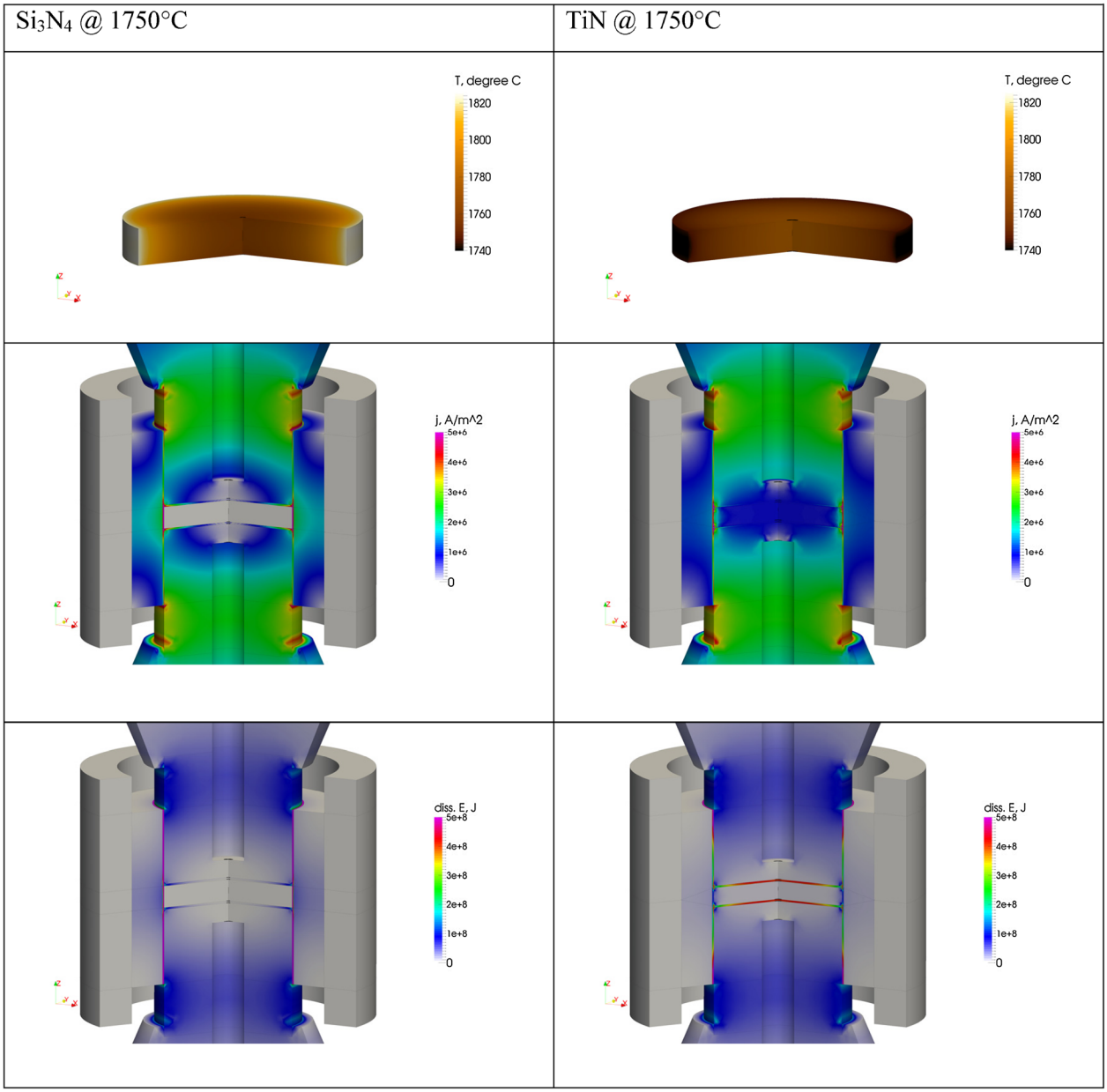

Fig. 5. Temperature, current density and dissipated energy distributions for an electrically insulating material (Si_3N_4) and an electrical conductor (TiN) after 5 min at 1750 °C (inner tool diameter: 40 mm).

4.4. Finite Element Modeling

Finite element modeling (FEM) is an important tool to predict distribution at the micro, meso, and macroscopic scales and temporal evolution of electrical potential and current, dissipated energy, temperature, stress (and ideally density and microstructure of the sintered sample) during a virtual FAST/SPS test. First simulations of the macroscopic temperature in current-assisted sintering were done in 1969[253] and in the early 1980s.[254] A detailed review of simulation works is given in ref.[4]

The tool geometry (including spacers, accommodation or separation foils, insulating felt), the temperature-dependent material properties (electrical resistivity, specific heat, thermal conductivity, bending and compressive strength, density, and emissivity) and the sintering profiles are required as input data for the electrical-thermal-mechanical coupled model. Contact resistances and their sensitivity to applied or resulting stresses are difficult to evaluate precisely, but should be taken into account to get realistic predictions[255] because they contribute to Joule heating. By varying the tool geometry and material data, a first optimization can be done before performing a series of tests. For example, the thickness and height of the die can be optimized to improve the temperature homogeneity within the sample.[13,14] An experimental validation has to be done to properly check the simulation results.[13,243,256] Many models have been developed, but most of the time only for tools of axisymmetric geometry, whose behavior can be therefore represented by 2D cross-sections.[13,256] Recently, more complex geometries have been presented in the literature.[257–259] In many cases, the sintering behavior is neglected and the material under consolidation is considered as a dense, elastic body. This can induce large errors in terms of stress level (a sintering materials being a viscous fluid). However, recent efforts have been done to implement specific constitutive sintering laws in FEM codes.[44,52,57,260–263]

As an example, FEM calculations are shown in Figure 5 for electrically insulating (Si_3N_4) and conductive (TiN) materials. The simulations are based on a FlexPDE transient model with coupled balance equations for thermal and electrical energy transport.[13] The moving mesh approach simulates the geometrical changes due to sintering. Beside conductive heat transport and convection from the moving parts of the tool, the model includes water-cooled pistons as an external boundary condition. Note the presence of graphite felt for insulation and graphite foils. The results of such a simulation have to be assessed by temperature measurements during FAST/SPS runs at two different positions at least. Figure 5 shows the temperature, current density, and dissipated (Joule) heat distribution after 5 min dwell time at 1750 °C (heating rate: 100 °C min^{-1}). The radial temperature distribution of the electrically conductive TiN is limited to 40 °C where the hottest area is located in the sample center. Although current flows through the sample, it does not lead to large Joule heating (dissipated energy) in its volume. Most of heat is produced in the parts of the piston, which are not inserted into the die as well as in the graphite foil. For the electrically insulating Si_3N_4, the radial temperature gradient is slightly larger (60 °C) with the hottest area close to the outer rim of the sample. No current is passing through the silicon nitride sample, which leads to a higher current density in the die close to sample. Especially, the graphite foil with its largely anisotropic electrical behavior provides a remarkable contribution to overall Joule heat production in the whole system. The current density distribution can be influenced by geometrical details of the pistons leading to a locally different dissipated energy production and therefore to a different temperature evolution.[13] Since most of the users working with FAST/SPS collect temperature data from only one measurement spot, such differentiated behavior is not well known and described in the literature. Anyway, the impact of large temperature gradient becomes relevant if FAST/SPS devices are up-scaled for the production of larger components.[9]

5. Conclusions

Field-assisted sintering technology/Spark plasma sintering is a versatile processing method for consolidation and synthesis of numerous new or improved materials. It enables the development of electrically conductive and non-conductive materials on demand at the lab scale (with processing cycles inclusive cooling down to room temperature of less than 1 h) or the rapid manufacturing of industrial products (with higher output, reduced energy costs). Sintering of refractory materials, dense nanostructured materials, non-equilibrium or functionally graded alloys, and composites are a few examples of success stories enabled by FAST/SPS.

Nevertheless, much research and development efforts are still ahead to lead FAST/SPS to maturity. On one hand, fundamental investigations of the transient mechanisms involved by high heating and cooling rates are required. Effects of electrical current/field on mass transport, reactivity, microstructure evolution, formability, and final properties need to be better understood. On the other hand, up scaling to large specimen dimensions and improved flexibility in terms of possible product geometries are needed. This requires the use of FEM calculations taking into account the real behavior of the materials.

Technological and scientific developments benefit from each other: for example, larger cooling rates allow "freezing" microstructures out of equilibrium. Finer, more stable microstructures enable superplastic deformation and low-temperature forming of dense materials. Coordinated research efforts and closer collaboration between research institutes and industry will be the necessary step to benefit from the full potential of FAST/SPS.

ADVANCED ENGINEERING MATERIALS

Received: August 17, 2013
Final Version: January 30, 2014
Published online: April 30, 2014

[1] Z. A. Munir, U. Anselmi-Tamburini, M. Ohyanagi, *J. Mater. Sci.* **2006**, *41*, 763.
[2] Z. A. Munir, D. V. Quach, M. Ohyanagi, *J. Am. Ceram. Soc.* **2011**, *94*, 1.
[3] J. E. Garay, *Annu. Rev. Mater. Res.* **2010**, *40*, 445.
[4] R. Orru, R. Licheri, A. M. Locci, A. Cincotti, G. Cao, *Mater. Sci. Eng. R* **2009**, *63*, 127.
[5] G. Cabouro, S. Chevalier, E. Gaffet, Y. Grin, F. Bernard, *J. Alloys Compd.* **2008**, *465*, 344.
[6] F. M. Zhang, F. Ahmed, J. Bednarcik, E. Burkel, *Phys. Status Solidi A-Appl. Mater. Sci.* **2012**, *209*, 2241.
[7] D. M. Hulbert, A. Anders, D. V. Dudina, J. Andersson, D. Jiang, C. Unuvar, U. Anselmi-Tamburini, A. K. Mukherjee, *J. Appl. Phys.* **2008**, *104*, 033305/1.
[8] D. M. Hulbert, A. Anders, J. Andersson, E. J. Lavernia, A. K. Mukherjee, *Scr. Mater.* **2009**, *60*, 835.
[9] J. Hennicke, H. U. Kessel, *CFI/Berichte DKG* **2004**, *81*, 11.
[10] M. Suárez, A. Fernández, J. L. Menéndez, R. Torrecillas, H. U. Kessel, J. Hennicke, R. Kirchner, T. Kessel, in *Sintering Applications* (Ed: B. Ertu), InTech, Croatia **2013**, pp. 319–342, Ch. 13.
[11] Z. A. Munir, W. Chen, U. Anselmi-Tamburini, J. E. Garay, J. R. Groza, *Mater. Sci. Eng. R* **2005**, *394*, 132.
[12] K. Vanmeensel, A. Laptev, O. Van der Biest, J. Vleugels, *Acta Mater.* **2007**, *55*, 1801.
[13] J. Räthel, M. Herrmann, W. Beckert, *CFI/Berichte DKG* **2008**, *85*, 13.
[14] S. Munoz, U. Anselmi-Tamburini, *J. Mater. Sci.* **2010**, *45*, 6528.
[15] A. G. Bloxam, *GB Patent* **1906**, No. 27, 002.
[16] G. Weintraub, H. Rush, *US Patent* **1913**, No. 1,071,488.
[17] K. Inoue, *US Patent* **1966**, No. 3,250,892.
[18] R. W. Boesel, *Mater. Eng.* **1969**, *70*, 32.
[19] R. W. Boesel, *Powder Metall.* **1971**, *3*, 38.
[20] R. W. Boesel, *Metal Prog.* **1971**, *99*, 74.
[21] C. G. Goetzel, *Mod. Dev. Powder Metall.* **1971**, *4*, 425.
[22] C. G. Goetzel, *Metals Eng. Q.* **1971**, *11*(2), 53.
[23] C. G. Goetzel, V. S. Marchi, *Powder Metall. Int.* **1971**, *3*, 80.
[24] S. Grasso, Y. Sakka, G. Maizza, *Sci. Technol. Adv. Mater.* **2009**, *10*, 053001.
[25] M. N. Rahaman, *Ceramic Processing and Sintering*, 2nd ed., Marcel Dekker, Inc., New York **2003**.
[26] O. Guillon, in *Sintering: Mechanisms of Convention Nanodensification and Field Assisted Processes* (Eds: R. Castro, K. van Benthem), Springer, Berlin/Heidelberg **2012**, pp. 195–213, Ch. 9.
[27] M. F. Ashby, *Acta Metall.* **1972**, *20*, 887.
[28] R. Chaim, M. Margulis, *Mater. Sci. Eng. A-Struct.* **2005**, *407*, 180.
[29] D. Salamon, M. Eriksson, M. Nygren, Z. Shen, *Sci. Technol. Adv. Mater.* **2012**, *13*, 015005.
[30] G. Bernard-Granger, N. Monchalin, C. Guizard, *Mater. Lett.* **2008**, *62*, 4555.
[31] G. Bernard-Granger, A. Addad, G. Fantozzi, G. Bonnefont, C. Guizard, D. Vernat, *Acta Mater.* **2010**, *58*, 3390.
[32] J. Langer, M. J. Hoffmann, O. Guillon, *Acta Mater.* **2009**, *57*, 5454.
[33] J. Langer, M. J. Hoffmann, O. Guillon, *J. Am. Ceram. Soc.* **2011**, *94*, 24.
[34] R. Marder, R. Chaim, C. Estournès, *Mater. Sci. Eng. A* **2010**, *527*, 1577.
[35] R. Chaim, *Mater. Sci. Eng. A-Struct.* **2007**, *443*, 25.
[36] J. Hu, Z. Shen, *Acta Mater.* **2012**, *60*, 6405.
[37] M. Herrmann, Z. Shen, I. Schulz, J. Hu, B. Jancar, *J. Mater. Res.* **2010**, *25*, 2354.
[38] H. Kessel, J. Hennicke, J. Schmidt, T. Weißgärber, B. Kieback, M. Herrmann, J. Räthel, *Pulvermetall.Wiss . Praxis* **2006**, *22*, 201.
[39] J. Hao, X. Wang, R. Chen, Z. Gui, L. Li, *J. Am. Ceram. Soc.* **2004**, *87*(7), 1404.
[40] L. D. Zhao, B. P. Zhang, J. F. Li, H. L. Zhang, W. S. Liu, *Solid State Sci.* **2008**, *10*, 651.
[41] U. Anselmi-Tamburini, J. E. Garay, Z. A. Munir, *Scr. Mater.* **2006**, *54*, 823.
[42] S. Grasso, B. N. Kim, C. Hu, G. Maizza, Y. Sakka, *J. Am. Ceram. Soc.* **2010**, *93*, 2460.
[43] S. Grasso, H. Yoshida, H. Porwala, Y. Sakka, M. Reece, *Ceram. Int.* **2013**, *39*, 3243.
[44] E. Olevsky, S. Y. Kandukuri, L. Froyen, *J. Appl. Phys.* **2007**, *102*, 114913/1.
[45] D. V. Quach, H. Avila-Paredes, S. Kim, M. Martin, Z. A. Munir, *Acta Mater.* **2010**, *58*, 5022.
[46] Z. J. Shen, M. Johnsson, Z. Zhao, M. Nygren, *J. Am. Ceram. Soc.* **2002**, *85*, 1921.
[47] Y. Zhou, K. Hirao, Y. Yamauchi, S. Kanzaki, *J. Eur. Ceram. Soc.* **2004**, *24*, 3465.
[48] O. Guillon, J. Langer, *J. Mater. Sci.* **2010**, *45*, 5191.
[49] S. Schwarz, A. M. Thron, J. Rufner, K. v. Benthem, O. Guillon, *J. Am. Ceram. Soc.* **2012**, *95*, 2451.
[50] T. B. Holland, T. B. Tran, D. V. Quach, U. Anselmi-Tamburini, J. R. Groza, A. K. Mukherjee, *J. Eur. Ceram. Soc.* **2012**, *32*, 3675.
[51] M. Herrmann, J. Räthel, A. Bales, K. Sempf, I. Sigalas, M. Höhn, *J. Eur. Ceram. Soc.* **2009**, *29*, 2611.
[52] E. Olevsky, L. Froyen, *J. Am. Ceram. Soc.* **2009**, *92*, S122.
[53] T. B. Holland, U. Anselmi-Tamburini, D. V. Quach, T. B. Tran, A. K. Mukherjee, *J. Eur. Ceram. Soc.* **2012**, *32*, 3667.
[54] A. V. Kuzmov, E. A. Olevsky, E. V. Alexandrova, *Powder Metall. Metal Ceram.* **2012**, *12/11*, 50.
[55] Z. A. Munir, D. V. Quach, M. Ohyanagi, in *Sintering: Mechanisms of Convention Nanodensification and Field Assisted Processes* (Eds: R. Castro, K. van Benthem), Springer, Berlin/Heidelberg **2012**, pp. 137–158, Ch. 7.
[56] U. Anselmi-Tamburini, G. Spinolo, F. Maglia, I. Tredici, T. B. Holland, A. K. Mukherjee, in *Sintering: Mechanisms*

of Convention Nanodensification and Field Assisted Processes (Eds: R. Castro, K. van Benthem), Springer, Berlin/Heidelberg **2012**, pp. 159–193, Ch. 8.
[57] B. McWilliams, A. Zavaliangos, *J. Mater. Sci.* **2008**, *43*, 5031.
[58] D. Schwesig, G. Schierning, R. Theissmann, N. Stein, N. Petermann, H. Wiggers, R. Schmechel, D. E. Wolf, *Nanotechnology* **2011**, *22*, 135601.
[59] A. Becker, S. Angst, A. Schmitz, M. Engenhorst, J. Stoetzel, D. Gautam, H. Wiggers, D. E. Wolf, G. Schierning, R. Schmechel, *Appl. Phys. Lett.* **2012**, *101*, 013113.
[60] M. Beekman, M. Baitinger, H. Borrmann, W. Schnelle, K. Meier, G. S. Nolas, Y. Grin, *J. Am. Chem. Soc.* **2009**, *131*, 9642.
[61] R. Raj, M. Cologna, J. S. C. Francis, *J. Am. Ceram. Soc.* **2011**, *94*, 1941.
[62] S. D. Antolovich, H. Conrad, *Mater. Manuf. Processes* **2004**, *19*, 587.
[63] T. B. Holland, U. Anselmi-Tamburini, D. V. Quach, T. B. Tran, A. K. Mukherjee, *J. Eur. Ceram. Soc.* **2012**, *32*, 3659.
[64] J. A. Varela, O. J. Whittemore, E. Longo, *Ceram. Int.* **1990**, *16*, 177.
[65] M. A. Thompson, M. P. Harmer, *J. Am. Ceram. Soc.* **1993**, *76*, 2248.
[66] L. Perazolli, J. A. Varela, E. R. Leite, E. Longo, *Mater. Sci. Forum* **1999**, *299–300*, 134.
[67] Y. K. Paek, K. Y. Eun, S. J. L. Kang, *J. Am. Ceram. Soc.* **1988**, *71*, 380.
[68] C. Nivot, F. Valdivieso, *Ceram. Int.* **2008**, *34*, 1595.
[69] H. Yoshida, K. Hiraga, T. Yamamoto, *Mater . Trans.* **2009**, *50*, 1032.
[70] J. G. Fisher, S. J. L. Kang, *J. Eur. Ceram. Soc.* **2009**, *29*, 2581.
[71] S. M. An, S. J. L. Kang, *Acta Mater.* **2011**, *59*, 1964.
[72] S. K. Biswas, F. L. Riley, *Mater. Chem. Phys.* **2001**, *67*, 175.
[73] N. Claussen, R. Wagner, L. J. Gauckler, G. Petzow, *J. Am. Ceram. Soc.* **1978**, *61*, 369.
[74] S. Jauregi, F. Fernandez, R. H. Palma, V. Martinez, J. J. Urcola, *Metall. Trans. A* **1992**, *23*, 389.
[75] J. G. Noudem, S. Quetel-Weben, R. Retoux, G. Chevallier, C. Estournes, *Scr. Mater.* **2013**, *68*, 949.
[76] A. Recnik, J. Bruley, W. Mader, D. Kolar, M. Ruhle, *Philos. Mag. B* **1994**, *70*, 1021.
[77] A. Navrotsky, *Int. J. Quantum Chem.* **2009**, *109*, 2647.
[78] J. L. Hebrard, P. Nortier, *J. Am. Ceram. Soc.* **1990**, *73*, 79.
[79] C. Han, A. Aksay, O. J. Whittemore, in *Advances in Materials Characterization II*, Plenum Press, New York **1985**, pp. 339–347.
[80] J. A. Varela, O. J. Whittemore, in *Sintering – Trajectory and Practice*, Elevier, Amsterdam, The Netherlands **1985**, p. 439.
[81] P. F. Eastman, I. B. Cutler, *J. Am. Ceram. Soc.* **1966**, *49*, 526.
[82] K. Hamano, K. Asano, Y. Akiyama, Z. Nakagawa, *Rep. Res. Lab. Mater.* **1979**, *4*, 59.
[83] B. K. Yoon, E. Y. Chin, S. J. L. Kang, *J. Am. Ceram. Soc.* **2008**, *91*, 4121.
[84] R. L. Coble, *J. Am. Ceram. Soc.* **1962**, *45*, 123.
[85] S. J. L. Kang, K. J. Yoon, *J. Eur. Ceram. Soc.* **1989**, *5*, 135.
[86] Z. Z. Fang, *Sintering of Advanced Materials*, Woodhead Publishing Limited, Sawston, Cambridge, UK **2010**.
[87] P. Angerer, L. G. Yu, K. A. Khor, G. Korb, I. Zalite, *J. Eur. Ceram. Soc.* **2005**, *25*, 1919.
[88] J. Langer, D. V. Quach, J. R. Groza, O. Guillon, *Int. J. Appl. Ceram. Technol.* **2011**, *8*, 1459.
[89] D. T. Jiang, A. K. Mukherjee, *Scr. Mater.* **2011**, *64*, 1095.
[90] Tietz, W. Wilson, *Behavior and Properties of Refractory Metals*, Stanford University Press, Stanford **1965**.
[91] A. Koutsospyros, W. Bradia, C. Christodoulatos, D. Dermatas, N. Strigul, *J. Hazardous Mater.* **2006**, *136*, 1.
[92] O. El-Atwani, V. Quach, M. Efe, P. R. Cantwell, B. Heim, B. Schultz, E. Stach, J. R. Groza, J. P. Allain, *Mater. Sci. Eng. A* **2011**, *528*, 5670.
[93] M. Yao, Z. Zhangjian, T. Jun, L. Ming, *Rare Metal. Mater. Eng.* **2011**, *40*, 4.
[94] H. Li, W. Pan, W. Zhang, S. Huang, H. Wu, *Adv. Funct. Mater.* **2013**, *23*, 209.
[95] K. Hu, X. Li, S. Qu, Y. Li, *Metall. Mater. Trans. A* **2013**, *44A*, 923.
[96] P. Angerer, E. Neubauer, L. G. Yu, K. A. Khor, *Int. J. Refrac. Met. Hard Mater.* **2007**, *25*, 280.
[97] R. Wiedemann, U. Martin, H. J. Seifert, A. Muller, *Int. J. Refrac. Met. Hard Mater.* **2010**, *28*, 550.
[98] P. Angerer, J. Wosik, E. Neubauer, L. G. Yu, G. E. Nauer, K. A. Khor, *Int. J. Refrac. Met. Hard Mater.* **2009**, *27*, 105.
[99] C. C. Koch, *Mater. Sci. Eng. A* **1998**, *244*, 39.
[100] T. Novoselova, S. Malinov, W. Sha, *Intermetallics* **2003**, *11*, 491.
[101] X. Li, A. Chiba, M. Sato, S. Takashash, *J. Alloys Compd.* **2002**, *336*, 232.
[102] G. Cao, L. Geng, Z. Zheng, M. Naka, *Intermetallics* **2007**, *15*, 1672.
[103] W. Liu, M. Naka, *Scr. Mater.* **2003**, *48*, 1225.
[104] T. Skyba, P. Hausild, M. Karlik, K. Vanmeensel, J. Vleugels, *Intermetallics* **2010**, *18*, 1410.
[105] S. Paris, E. Gaffet, F. Bernard, Z. A. Munir, *Scr. Mater.* **2004**, *50*, 691.
[106] Y. Liu, W. Liu, *J. Alloys Compd.* **2007**, *440*, 154.
[107] S. Xiao, J. Tian, L. Xu, Y. Chen, H. Yu, J. Han, *Trans. Nonferrous Mater. Soc. China* **2009**, *19*, 1423.
[108] Y. Y. Cheng, H. B. Yu, D. L. Zhang, L. H. Chai, *Mater. Sci. Eng. A* **2009**, *525*, 166.
[109] R. Orru, R. Licheri, A. Locci, A. Cincotti, G. Cao, *Mater. Sci. Eng. R* **2009**, *63*, 127.
[110] J. Meng, C. Jia, Q. Ile, *Mater. Sci. Eng. A* **2006**, *434*, 246.

[111] T. Grosdidier, G. Ji, F. Bernard, E. Gaffet, Z. A. Munir, S. Launois, *Intermetallics* **2006**, *14*, 1208.
[112] G. Ji, T. Grosdidier, N. Bozzolo, S. Launois, *Intermetallics* **2007**, *15*, 108.
[113] W. G. Fahrenholtz, G. E. Hilmas, I. G. Talmy, J. A. Zaykoski, *J. Am. Ceram. Soc.* **2007**, *90*, 1347.
[114] E. Wuchina, E. Opila, M. Opeka, W. Fahrenholtz, I. Talmy, *Electrochem. Soc. Inter.* **2007**, 30.
[115] A. Paul, D. Jayaseelan, S. Venugopal, E. Zapata-Solvas, J. Binner, B. Vaidhyanathan, A. Heaton, P. Brown, W. E. Lee, *Am. Ceram. Soc. Bull.* **2008**, *91*, 22.
[116] S. Guo, *J. Eur. Ceram. Soc.* **2009**, *29*, 995.
[117] E. Zapata-Solvas, D. D. Jayaseelan, H. T. Lin, P. Brown, W. E. Lee, *J. Eur. Ceram. Soc.* **2013**, *33*, 1373.
[118] Z. H. Zhang, X. B. Shen, F. C. Wang, S. K. Lee, L. Wang, *Mater. Sci. Eng. A* **2010**, *527*, 5947.
[119] H. Fu, W. Peng, T. Gao, *Mater. Chem. Phys.* **2009**, *115*, 789.
[120] X. Zhang, G. E. Hilmas, W. G. Farenholtz, *Mater. Sci. Eng. A* **2009**, *501*, 37.
[121] Y. Li, K. Hu, X. Li, X. Ai, S. Qu, *Mater. Sci. Eng. A* **2013**, *573*, 245.
[122] M. Thompson, W. G. Fahrenholtz, G. Hilmas, *J. Am. Ceram. Soc.* **2011**, *94*, 429.
[123] V. Zamora, A. L. Ortiz, F. Guiberteau, M. Nygren, *J. Eur. Ceram. Soc.* **2012**, *32*, 271.
[124] L. Liu, F. Ye, Y. Zhou, *Mater. Sci. Eng. A* **2011**, *528*, 4710.
[125] H. Liu, L. Liu, F. Ye, Z. Zhang, Y. Zhou, *J. Eur. Ceram. Soc.* **2012**, *32*, 3617.
[126] D. Sciti, G. Bonnefont, G. Fantozzi, L. Silvestroni, *J. Eur. Ceram. Soc.* **2010**, *30*, 3253.
[127] A. Bellosi, F. Monteverde, D. Sciti, *Int. Appl. Ceram. Technol.* **2006**, *3*, 32.
[128] W. G. Fahrenholtz, G. E. Hilmas, *Int. Mater. Rev.* **2012**, *57*, 61.
[129] M. Gasch, D. Ellerby, E. Irby, S. Beckman, M. Gusman, S. Johnson, *J. Mater. Sci.* **2004**, *39*, 5925.
[130] T. Mizuguchi, S. Guo, Y. Kagawa, *Ceram. Int.* **2010**, *36*, 943.
[131] A. Krell, T. Hutzler, J. Klimke, *J. Eur. Ceram. Soc.* **2009**, *29*, 207.
[132] Y. Kodera, C. L. Hardin, J. E. Garay, *Scr. Mater.* **2013**, *69*, 149.
[133] R. Chaim, M. Kalina, J. Z. Shen, *J. Eur. Ceram. Soc.* **2007**, *27*, 3331.
[134] N. Frage, S. Kalabukhov, N. Sverdlov, V. Kasiyan, A. Rothman, M. P. Dariel, *Ceram. Int.* **2012**, *38*, 5513.
[135] G. Spina, G. Bonnefont, P. Palmero, G. Fantozzi, J. Chevalier, L. Montanaro, *J. Eur. Ceram. Soc.* **2012**, *32*, 2957.
[136] E. H. Perilla, Y. Kodera, J. E. Garay, *Mater. Sci. Eng. B* **2012**, *177*, 1178.
[137] H. Zhang, B. N. Kim, K. Morita, H. Yoshida, K. Hiraga, Y. Sakka, *J. Am. Ceram. Soc.* **2011**, *94*, 3206.
[138] R. Chaim, Z. Shen, M. Nygren, *J. Mater. Res.* **2004**, *19*, 2527.
[139] K. Morita, B. N. Kim, H. Yoshida, K. Hiraga, *J. Am. Ceram. Soc.* **2009**, *92*, 1208.
[140] G. Bonnefont, G. Fantozzi, S. Trombert, L. Bonneau, *Ceram. Int.* **2012**, *38*, 131.
[141] U. Anselmi-Tamburini, J. N. Woolman, Z. A. Munir, *Adv. Funct. Mater.* **2007**, *17*, 3267.
[142] L. An, I. Akihiko, T. Goto, *J. Eur. Ceram. Soc.* **2012**, *32*, 3097.
[143] B. N. Kim, H. Keijiro, K. Morita, H. Yoshida, T. Miyazaki, Y. Kagawa, *Acta Mater.* **2009**, *57*, 1319.
[144] S. Grasso, C. Hu, G. Maizza, B. N. Kim, Y. Sakka, *J. Am. Ceram. Soc.* **2011**, *94*, 1405.
[145] N. Roussel, L. Lallemant, J. Y. Chane-Ching, S. Guillemet-Fritsch, B. Durand, V. Garnier, G. Bonnefont, G. Fantozzi, L. Bonneau, S. Trombert, D. Garcia-Guterriez, *J. Am. Ceram. Soc.* **2013**, *96*, 1039.
[146] D. Jiang, D. M. Hulbert, U. Anselmi-Tamburini, T. Ng, D. Land, A. K. Muherjee, *J. Am. Ceram. Soc.* **2008**, *91*, 151.
[147] U. Anselmi-Tamburini, J. N. Woolman, Z. A. Munir, *Adv. Funct. Mater.* **2007**, *17*, 3267.
[148] M. Eriksson, Y. Liu, H. Jiangfeng, L. Gao, M. Nygren, Z. Shen, *J. Eur. Ceram. Soc.* **2011**, *31*, 1533.
[149] L. Lallemant, G. Fantozzi, V. Garnier, G. Bonnefont, *J. Eur. Ceram. Soc.* **2012**, *32*, 2909.
[150] L. An, I. Akihiko, T. Goto, *J. Am. Ceram. Soc.* **2011**, *94*, 3851.
[151] G. Bernard-Granger, N. Benameur, C. Guizard, M. Nygren, *Scr. Mater.* **2009**, *60*, 164.
[152] S. R. Casolco, J. Xu, J. E. Garay, *Scr. Mater.* **2008**, *58*, 516.
[153] I. Schulz, M. Herrmann, I. Endler, I. Zalite, B. Speisser, J. Kreusser, *Nano Lubrication Sci.* **2009**, *21*, 69.
[154] F. Maglia, I. G. Tredici, U. Anselmi-Tamburini, *J. Eur. Ceram. Soc.* **2013**, *33*, 1045.
[155] I. W. Chen, X. H. Wang, *Nature* **2000**, *404*, 168.
[156] S. Schwarz, O. Guillon, *J. Eur. Ceram. Soc.* **2013**, *33*, 637.
[157] O. Zgalat-Lozynskyy, M. Herrmann, A. Ragulya, *J. Eur. Ceram. Soc* **2011**, *31*, 809.
[158] R. Chaim, M. Levin, A. Shlayer, C. Estournes, *Adv. Appl. Ceram.* **2008**, *107*, 159.
[159] I. G. Tredici, F. Maglia, M. Dapiaggi, G. Spinolo, U. Anselmi-Tamburini, *J. Eur. Ceram. Soc.* **2012**, *32*, 343.
[160] F. Maglia, M. Dapiaggi, I. G. Tredici, U. Anselmi-Tamburini, *Nanosci. Nanotechnol. Lett.* **2012**, *4*, 205.
[161] Z. Zhao, V. Buscaglia, M. Viviani, M. T. Buscaglia, L. Mitoseriu, A. Testino, M. Nygren, M. Johnsson, P. Nanni, *Phys. Rev. B* **2004**, *70*, 024107.
[162] X. Deng, X. Wang, H. Wen, A. Kang, Z. L. Gui Li, *J. Am. Ceram. Soc.* **2006**, *89*, 1059.
[163] J. Liu, Z. Shen, W. Yao, Y. Zhao, A. K. Mukherjee, *Nanotechnology* **2010**, *21*, 075706.
[164] T. Hungría, H. Amorín, M. Algueró, A. Castro, *Scr. Mater.* **2011**, *64*, 97.
[165] M. Algueró, T. Hungría, H. Amorín, J. Ricote, J. Galy, A. Castro, *Small* **2007**, *3*, 1906.

[166] S. Imine, F. Schoenstein, S. Mercone, M. Zaghrioui, N. Bettahar, N. Jouini, *J. Eur. Ceram. Soc.* **2001**, *31*, 2943.
[167] R. Valenzuela, Z. Beji, F. Herbst, S. Ammar, *J. Appl. Phys.* **2011**, *109*, 07A329-1–323.
[168] K. Nielsch, J. Bachmann, J. Kimling, H. Böttner, *Adv. Energy Mater.* **2011**, *1*, 713.
[169] T. Noguchi, in *XVI International Conference on Thermoelectrics*, **1997**.
[170] S. Yoneda, in *XVI International Conference on Thermoelectrics*, **1997**.
[171] I. Matsubara, R. Funahashi, T. Takeuchi, S. Sodeoka, *J. Appl. Phys.* **2001**, *90*, 462.
[172] Y. Liu, Y. Lin, Z. Shi, C. W. Nan, Z. Shen, *J. Am. Ceram. Soc.* **2005**, *88*, 1337.
[173] B. Poudel, Q. Hao, Y. Ma, Y. Lan, A. Minnich, B. Yu, X. Yan, D. Wang, A. Muto, D. Vashaee, X. Chen, J. Liu, M. S. Dresselhaus, G. Chen, Z. Ren, *Science* **2008**, *320*, 634.
[174] G. Joshi, H. Lee, Y. Lan, X. Wang, G. Zhu, D. Wang, R. W. Gould, D. C. Cuff, M. Y. Tang, M. S. Dresselhaus, G. Chen, Z. Ren, *Nano Lett.* **2008**, *8*, 4670.
[175] X. W. Wang, H. Lee, Y. C. Lan, G. H. Zhu, G. Joshi, D. Z. Wang, J. Yang, A. J. Muto, M. Y. Tang, J. Klatsky, S. Song, M. S. Dresselhaus, G. Chen, Z. F. Ren, *Appl. Phys. Lett.* **2008**, *93*, 193121.
[176] G. Schierning, R. Theissmann, N. Stein, N. Petermann, A. Becker, M. Engenhorst, V. Kessler, M. Geller, A. Beckel, H. Wiggers, R. Schmechel, *J. Appl. Phys.* **2011**, *110*, 113515.
[177] Y. Kinemuchi, M. Mikami, K. Kobayashi, K. Watari, Y. Hotta, *J. Electron. Mater.* **2010**, *39*, 2059.
[178] Y. Kinemuchi, H. Nakano, M. Mikami, K. Kobayashi, K. Watari, Y. Hotta, *J. Appl. Phys.* **2010**, *108*, 053721.
[179] M. Backhaus-Ricoult, J. Rustad, D. Vargheese, I. Dutta, K. Work, *J. Electron. Mater.* **2012**, *41*, 1636.
[180] Y. Wang, K. Fujinami, R. Zhang, C. Wan, N. Wang, Y. Ba, K. Koumoto, *Appl. Phys. Express* **2010**, *3*, 031101.
[181] M. Zhou, J. F. Li, T. Kita, *J. Am. Chem. Soc.* **2008**, *130*, 4527.
[182] K. Biswas, J. He, I. D. Blum, C. I. Wu, T. P. Hogan, D. N. Seidman, V. P. Dravid, M. G. Kanatzidis, *Nature* **2012**, *489*, 414.
[183] M. B. Bever, P. F. Duwez, *Mater. Sci. Eng.* **1972**, *10*, 1.
[184] A. Neubrand, J. Rödel, *Z. Metallkd.* **1997**, *88*, 358.
[185] B. Kieback, A. Neubrand, H. Riedel, *Mater. Sci. Eng. A* **2003**, *362*, 81.
[186] M. Nygren, Z. Shen, *Solid State Sci.* **2003**, *5*, 125.
[187] H. Guo, K. A. Khor, Y. C. Boey, X. Miao, *Biomaterials* **2003**, *24*, 667.
[188] X. Zhang, W. Li, C. Hong, W. Han, J. Han, *Scr. Mater.* **2008**, *59*, 1214.
[189] H. Feng, Q. Meng, Y. Zhou, D. Jia, *Mater. Sci. Eng. A* **2005**, *397*, 92.
[190] W. M. Rubio, G. H. Paulino, E. N. Silva, *Mater. Des.* **2012**, *41*, 255.
[191] G. Jin, M. Takeuchi, S. Honda, T. Nishikawa, H. Awaji, *Mater. Chem. Phys.* **2005**, *89*, 238.
[192] H. Mishina, Y. Inumaru, K. Kaitoku, *Mater. Sci. Eng. A* **2008**, *475*, 141.
[193] C. E. J. Dancer, M. Achintha, C. J. Salter, J. A. Fernie, R. I. Todd, *Scr. Mater.* **2012**, *67*, 281.
[194] M. Belmonte, J. Gonzalez-Julian, P. Miranzo, M. I. Osendi, *Acta Mater.* **2009**, *57*, 2607.
[195] C. Hong, X. Zhang, W. Li, J. Han, S. Meng, *Mater. Sci. Eng. A* **2008**, *498*, 437.
[196] Y. Liu, Z. Jin, *Ceram. Int.* **2012**, *38*, 217.
[197] Z. Zhang, X. Shen, C. Zhang, S. Wie, S. Lee, F. Wang, *Mater. Sci. Eng. A* **2013**, *565*, 326.
[198] S. Wei, Z. Zhang, X. Shen, F. Wang, M. Sun, R. Yang, S. Lee, *Comp Mater. Sci.* **2012**, *60*, 168.
[199] Z. Shen, M. Nygren, *Key Eng. Mater.* **2003**, *247*, 79.
[200] Z. Shen, M. Nygren, *J. Eur. Ceram. Soc.* **2001**, *21*, 611.
[201] Z. Shen, M. Nygren, *J. Mater. Chem.* **2001**, *11*, 204.
[202] M. Herrmann, J. Räthel, I. Schulz, *Interceram* **2009**, *58*, 109
[203] A. Schönecker, in *Final Report of the IGF Project "Piezo FAST"*, BR 09 453 IKTS/DKG **2010**.
[204] T. Schubert, B. Lorenz, J. Steger, T. Weissgärber, R. Neugebauer, B. Kieback, in *Challenge for the Next Generation. Powder Metallurgy World Congress*, Yokohama, Japan **2012**.
[205] F. Zhang, M. Reich, O. Kessler, E. Burkel, *Mater. Today* **2013**, *16*, 192.
[206] M. Herrmann, B. Matthey, S. Höhn, I. Kinski, D. Rafaja, A. Michaelis, *J. Eur. Ceram. Soc.* **2011**, *32*, 1915.
[207] S. Grasso, C. Hu, G. Maizza, Y. Sakka, *J. Am. Ceram. Soc.* **2011**, *94*, 1.
[208] B. Yaman, H. Mandal, *Mater. Lett.* **2009**, *63*, 1041.
[209] M. Hotta, T. Goto, *J. Am. Ceram. Soc.* **2009**, *92*, 1684.
[210] M. Hotta, T. Goto, *J. Ceram. Soc. Jpn.* **2008**, *116*, 744.
[211] F. Ye, Z. Hou, H. Zhang, L. Liu, Y. Zhou, *Mater. Sci. Eng. A* **2010**, *527*, 4723.
[212] J. Garrett, I. Sigalas, M. Herrmann, E. Olivier, J. OConnell, *J. Eur. Ceram. Soc.* **2013**, *33*, 2191.
[213] R. Holke, V. Richter, W. Böhlke, F. Weiland, G. Barbier, in *EURO PM2006, Conference & Exhibition*, Ghent, Belgium **2004**.
[214] J. Räthel, F. Hanspach, M. Herrmann, *Poster, High Pressure Symposium*, Freiberg **2012**.
[215] C. Laurent, G. Chevallier, A. Weibel, A. Peigney, C. Estournès, *Carbon* **2008**, *46*, 1812.
[216] G. D. Zhan, J. D. Kuntz, J. L. Wan, A. K. Mukherjee, *Nat. Mater.* **2003**, *2*, 38.
[217] K. Ahmad, W. Pan, *Ceram. Eng. Sci. Proc.* **2009**, *29*, 49.
[218] L. Kumari, T. Zhang, G. H. Du, W. Z. Li, Q. W. Wang, A. Datye, K. H. Wu, *Comp. Sci. Technol.* **2008**, *68*, 2178.
[219] W. B. Tian, Y. M. Kan, G. J. Zhang, P. L. Wang, *Mater. Sci. Eng. A* **2008**, *487*, 568.
[220] M. I. Osendi, F. Gautheron, P. Miranzo, M. Belmonte, *J. Nanosci. Nanotechnol.* **2009**, *9*, 6188.

[221] E. L. Corral, H. Wang, J. Garay, Z. Munir, E. V. Barrera, *J. Eur. Ceram. Soc.* **2011**, *31*, 391.
[222] M. Mazaheri, D. Mari, Z. R. Hesabi, R. Schaller, G. Fantozzi, *Compos. Sci. Technol.* **2011**, *71*, 939.
[223] O. Malek, J. Gonzalez-Julian, J. Vleugels, W. Vanderauwera, B. Lauwers, M. Belmonte, *Mater. Today* **2011**, *14*, 496.
[224] F. Zhang, F. Ahmedb, G. Holzhüter, E. Burkel, *J. Cryst. Growth* **2012**, *340*, 1.
[225] F. Zhang, F. Ahmedb, J. Bednarcik, E. Burkel, Phys., *Status Solidi A Mater. Sci.* **2012**, *209*, 2241.
[226] H. U. Kessel, *CFI/Berichte DKG* **2009**, *86*(10), E145.
[227] M. Tokita, *KORUS 2000, The Korea-Russia International Symposium on Science and Technology* **2000**, *3*, pp. 251–256.
[228] M. Tokita, *Mater. Sci. Forum* **1999**, *308–311*, 83.
[229] H. Ishida, *Patent JP2004068089* **2000**.
[230] E.W. Engle, *Patent US2195297* **1938**.
[231] M. T. Simnad (inventor), *Patent US3182102* **1965**.
[232] X. Li, Y. Ye, Y. Tang, S. Qu, *Mater. Trans.* **2010**, *51*, 1308.
[233] J. Hennicke, H. Kessel, R. Kirchner, *GCFI/Berichte DKG* **2011**, *88*, D21.
[234] K. Morsi, A. El-Desouky, B. Johnson, A. Mar, S. Lanka, *Appl. Sci. Manuf.* **2009**, *41*, 32.
[235] Z. Shen, H. Peng, M. Nygren, *Adv. Mater.* **2003**, *15*, 1006.
[236] K. A. Vanmeensel Laptev, H. Sheng, I. Tkachenko, O. Van der Biest, J. Vleugels, *Acta Mater.* **2013**, *61*, 2376.
[237] G. F. Taylor (inventor), *Patent US1918064* **1933**.
[238] G. F. Taylor (inventor), *Patent US1991233* **1935**.
[239] J. Schmidt, T. Hutsch, T. Wießgärber, B. Kieback, *Pulvermetallurgie in Wissenschaft und Praxis*, Vol. *24*, Heimdall Verlag, Rheine, Germany **2008**, pp. 33–54.
[240] J. Schmidt, A. Knote, M. Armbrüster, T. Weißgärber, B. Kieback, *Diamante, Appl. Tecnol.* **2011**, *17*, 35.
[241] M. Tokita, *Contributed Article for 1st Russia–Japan Workshop*, Moskow **2013**.
[242] H. U. Kessel, J. Hennicke, T. Kessel, *CFI-Ceram. Forum Int.* **2010**, *87*, E23.
[243] G. A. Weissler, *Int. J. Powder Metall. Powder Technol.* **1981**, *17*, 107.
[244] F. V. Lenel, *J. Metals* **1955**, *7*, 158.
[245] A. I. Raichenko, L. V. Zabolotnyi, O. L. Ryabinina, V. V. Pushkarev, *Poroshk. Metall.* **1980**, *213*, 6.
[246] M. Kamikawa, Y. Kano, *Patent JP2001226703* **2001**.
[247] M. Herrmann, I. Schulz, A. Bales, K. Sempf, S. Hoehn, *J. Eur. Ceram. Soc.* **2008**, *28*, 1049.
[248] J. Langer, D. V. Quach, J. R. Groza, O. Guillon, *Int. J. Appl. Ceram. Technol.* **2011**, *8*, 1459.
[249] T. Voisin, L. Durand, N. Karnatak, S. Le Gallet, M. Thomas, Y. Le Berre, J. F. Castagné, A. Couret, *J. Mater. Process. Technol.* **2013**, *213*, 269.
[250] M. Herrmann, Z. Shen, I. Schulz, J. Hu, B. Jancar, *J. Mater. Res.* **2010**, *25*, 2354.
[251] Z. A. Munir, U. Anselmi-Tamburini, S. Gennari, J. E. Garay, *Mater. Sci. Eng. R* **2005**, *394*, 139.
[252] Y. Wang, Z. Fu, *Mater. Sci. Eng. B* **2002**, *90*, 34.
[253] A. E. Vidoz, W. S. Rothwell, *Research Report – Lockheed Palo Alto Research Laboratory*, Materials Science Lab., Palo Alto, CA, USA **1969**.
[254] A. I. Raichenko, *Phys. Sinter.* **1973**, *5*, 215.
[255] A. Zavaliangos, J. Zhang, M. Krammer, J. R. Groza, *Mater. Sci. Eng. A* **2004**, *379*, 218.
[256] K. Vanmeensel, A. Laptev, J. Hennicke, J. Vleugles, O. Van den Biest, *Acta Mater.* **2005**, *53*, 4379.
[257] B. McWilliams, A. Zavaliangos, K. C. Cho, R. J. Dowding, *J. Metals* **2006**, *58*, 27.
[258] E. Olevsky, W. L. Bradbury, C. D. Haines, D. G. Martin, D. Kapoor, *J. Am. Ceram. Soc.* **2012**, *95*, 2406.
[259] E. Olevsky, C. Garcia-Cardona, W. L. Bradbury, C. D. Haines, D. G. Martin, D. Kapoor, *J. Am. Ceram. Soc.* **2012**, *95*, 2414.
[260] E. Olevsky, L. Froyen, *Scr. Mater.* **2006**, *55*, 1175.
[261] E. Olevsky, S. Kandukuri, L. Froyen, *Key Eng. Mater.* **2008**, *368–372*, 1580.
[262] C. Wolff, S. Mercier, H. Couque, A. Molinari, *Mech. Mater.* **2012**, *49*, 72.
[263] P. Mondalek, L. Silva, M. Bellet, *Adv. Eng. Mater.* **2011**, *13*, 587.

